Bachelor of Science Thesis (1985)
(Geology)
McMaster University
Hamilton, Ontario

PETROGRAPHY OF THE QUARTZ THOLEIITES FROM THE MISIONES PROVINCE, ARGENTINA

Author: Glenn M. Smelser

Supervisor: Dr. B.J. Burley

Number of Pages: 83

ACKNOWLEDGEMENTS

I would like to acknowledge the grateful assistance of a few of the many whose ideas and help have contributed throughout the year: Professor B.J. Burley for providing samples, thin sections and guidance; Otto Murdoch for his valuable assistance regarding sample preparation and analysis; Jack Whorwood for photomicrographs and special appreciation to Ethel Markus and the Hamilton Word Processing Centre for their time and effort in transforming my mass of computer paper notes into what you now see before your eyes.

TABLE OF CONTENTS

INTRODUCTION

The Paraná basalts of the Misiones Province in Argentina are remarkably similar with respect to their mineralogy and major element chemistry. This is quite remarkable when considering the vast geographic area these samples cover (a base map with sample locations is provided in the back flap). The areal extent of the Misiones Province is approximately 3000km^2 and sample localities separated by 300km may display a variation in their silica contents of only 1.5%. From a viewpoint considering the areal extent of some flood basalts, this is not at all uncommon but is what should be expected.

The basalts sampled from the Misiones Province are all typical quartz tholeiites with hypersthene appearing as rare phenocrysts but more commonly is a constituent of the glassy groundmass. The essential mineral in all these samples is a calcic plagioclase which accounts for approximately 40% of most samples. One inconsistency of these samples is the relative abundance and nature of the volcanic glassy matrix which is generally controlled by the rate of change in temperature as the magma is brought to the surface where it subsequently crystallizes. This volcanic glass: crystalline phase ratio, being a near surface phenomenon requires a parameter(s) that may account for variations of tholeiitic equilibration at shallow depths. A feasible conclusion to satisfy this observation is that the magma has issued out of numerous fissures, with each fissure providing unique physical parameters that will effect the abundance of late stage quench products such as volcanic glass.

To support this hypothesis is the abundance of dikes in the Misiones Province that could serve as fissures for the expulsion of the magma.

Therefore, it seems probable that these quartz tholeiites have all been derived from a common source rock and their mineralogical and chemical differences are attributed to their unique near surface environments in which they equilibrated.

THE GEOLOGICAL HISTORY OF THE PARANÁ BASIN, SOUTH AMERICA

The Paraná basalts are located in the Paraná basin in South America and cover vast areas of southwestern Brazil and portions of Uruguay, Paraguay and Argentina. The hydrographic basin of the Paraná River extends into the southern region of the Amazon River's drainage basin. Basalts or diabases (dolerites) are found extensively in this region which is a vast geosyncline bounded on all sides by outcrops of Pre-Cambrian or early Paleozoic basement complex of plutonic and metamorphic rocks. The major structural trends in this area are northeast-southwest and run in a subparallel orientation with the southern Brazil and Uruguay coastline, and to the major axis of the Paraná downfold. During the Pre-Cambrian or early Paleozoic era, the eastern region was bounded by a mountain range but all that remains today are small hill ranges, signifying the effectiveness of erosion that has operated in this region over geological time. Today the highest mountains and ridges are made of either folded and faulted metamorphic quartzites or bosslike masses of syenitic intrusives. (Baker)

During the lower Devonian epoch, much of the interior of South America was covered by a vast sea which resulted in the deposition of non-fossiliferous basal conglomerates, nearshore sandstones and alluvial deposits followed by Lower Devonian marine shales and sandstones. Erosion following this epoch removed a vast quantity of these lower Devonian marine sediments and possibly some older sediments forming the eastern and northern boundaries of the Paraná depositional basin.

Later sedimentation into the Paraná basin was dominantly of a continental origin although some marine brachiopods and molluscs (fresh-water and brackish-water forms) have been found in the Estrada Nova beds of both SãO Paulo and Paraná. Initial continental type deposits were alluvial sandstones and shales, coal beds and palustrine carbonaceous and bituminous shales located in the Brazilian states of SãO Paulo, Paraná, and Santa Catharina. These deposits compose the Rio Bonito beds and are found directly overlying the basement complex with little or no basal conglomerates present. The Rio Bonito is succeed by the Palermo shales which is a relatively thin formation. Next is the Iraty, a thin formation of bituminous shales interbedded with limestones and cherts which is interpreted as a fresh-water lake deposit. This depositional cycle was ended by the deposition of clays and some thin concretionary limestones, which developed a total thickness of 500m. This first depositional sequence ranges from the early Permian or Permo-Carboniferous era.

An erosional unconformity exists between the sequence just descried and the overlying red beds of the Rio de Rastro formation (approximately 100m thick). This formation is composed of shales, sandstones and a few conglomerates. Overlying this is the 225m thick SãO Bento formation composed of crossbedded sandstones and some conglomeratic beds.

The lower sheets of the Paraná basalts are often interbedded with the sandstones of the SãO Bento formation and are interpreted either as flow sheets with interbedded sandstones or

as intruded sills. These interbedded sandstone layers become progressively less abundant as the stratigraphic column is traversed and upper sandstone interbeds are generally confined to the margins of the original lava field.

The flows tend to display quite a variable nature ranging from vesicular to very dense flows containing columnar structures. This area is devoid of pyroclastic material and lacks evidence to support the validity that true volcanic activity has taken place although this evidence may have become obliterated as many of these rocks are so highly altered that their origin is uncertain. However, there is a very extensive fissure network by which the lava reached the surface which is verified by the vast number of dikes found in this area. The basalts and diabases (dolerites) have a composition that range from andesites and olivine-free augite-porphyrites to limburgites with abundant olivine.

The Paraná basalt lavas have been radiometrically dated, indicating eruption took place over a period ranging from the late Jurassic to mid-Cretaceous with peak activity in the early Cretaceous (Cordani and Vandoros, 1967). This epoch of basalt formation corresponds approximately to the break-up of Gondwanaland and the formation of the South Atlantic basin. This observation is supported by paleomagnetic data on the overlapping geomagnetic poles of South America and Africa during the late Paleozoic and early Mesozoic.

The Paraná basalts cover an extensive area of southwestern Brazil and portions of Uruguay, Paraguay and Argentina. Maack (1952) estimated that the Paraná basalts cover an area of approximately 1.2×10^6 km^2 but their original extent may have approached 2.0×10^6 km^2 but much of this has been removed by erosion during the Mesozoic and Cenozoic. Some physical characteristics of the Paraná basalts are listed in table 2.1 and are compared to other Pre-Tertiary basaltic plateaus.

Table 2.1
PHYSICAL ASPECTS OF FOUR PRE-TERTIARY BASALT PLATEAUS

Basalt Plateau	Age	Maximum and Average Thickness	Present and Possible Original Area	Approximate Volume	Flow Thickness
Paraná Basin	Late Jurassic to early Cretaceous 119-149 m.y.	1500-1800m ave. 650m	1,200,000 km^2 orig. 2,000,000km^2	650,000km^3	ave. 50m max. 100m
Karroo Province	Late Triassic to early Jurassic 166-206 m.y.	8000-9000m ave. 1000m	140,000Km^2 orig. 2,000,000km^2	?	ave. 10m (Lestho) sills to 1000m
Siberian Platform	Early Permian to Triassic (most early Triassic) 216-248 m.y.	3500m ave. 1000m	>1,500,000km^2	575,000km^3 (911,000km^3 including intrusions)	ave. 30m
Lake Superior Basin (Keween-awan)	Late Precambrian 1100-1120 m.y.	8000-12000m ave. 5000m	100,000km^2* orig.125,000km^2	>300,000km^3*	3-30m ave.25m max. 400m

* In Lake Superior area only; much greater with rest of mafic rocks of the Mid-continent Gravity High. (Cordani and Vandoros)

THE GENERATION OF BASALTIC MAGMA AND THE VIABILITY OF PERIDOTITE ACTING AS A SOURCE ROCK

Seismic investigations have revealed that the majority of the mantle is crystalline and models of basaltic magma generation must stipulate that the parental material be melted. The basic requirements for parental source rocks are:

1) it must be able to produce a liquid of basaltic composition without crystals or,

2) a later stage crystal-liquid mush from which a liquid of basaltic composition may be derived at relatively shallow depths.

Several parental materials have been considered as possible source rocks for basaltic magma, which can be divided into two basic categories:

1) parental material that have compositions similar to basalts which include amphibolite, hornblendite and eclogite and,

2) parental material that produces a basaltic magma due to partial melting which includes garnet peridotites.

Amphibolites are a proposed source rock for basaltic magma generation at high water pressures. Yoder and Tilley (1962) proposed that amphibolites could be generated from a basaltic or gabbroic source rock by the addition of water at high pressure and continuing laboratory research has verified their results. However, this process is limited to shallow depths due to amphiboles instability with increasing pressure (amphibole becomes unstable above 30kb which corresponds to approximately 100km). Bowen (1928) concluded that amphiboles do not play a

major role in the generation of common basaltic magmas, but their presence at shallow depths may modify fractionation trends.

Yoder and Tilley (1957) experimentally determined that basalts and gabbros are stable only at shallow depths (see figure 3.1) but could be converted to an eclogite assemblage by increasing pressure. The mineralogy of eclogites is characterized by abundant clinopyroxene, garnet, and minor amounts of hypersthene, quartz and kyanite. The conversion of basaltic mineral assemblages to yield eclogite assemblages at elevated pressures has been verified by several investigations based on:

1) laboratory experiments with combinations of simple end members.
2) the reactions of anorthite with forsterite and enstatite.
3) the breakdown of albite (Birch and LaComte, 1960) and,
4) the interaction of clinopyroxene with plagioclase (Kushiro, 1969).

Eclogites acting as a source rock for basaltic magmas does not necessitate that the entire source rock must be melted. Eclogites melt over a confined temperature range and each melt fraction is capable of producing a basaltic composition. A setback to this is that at certain depths, eclogite compositions may melt at higher temperatures than its host rock and would therefore be classified as a residuum rather than a source for basaltic magma generation.

This observation combined with the lack of olivine in eclogites which appears to be an important phase in parental

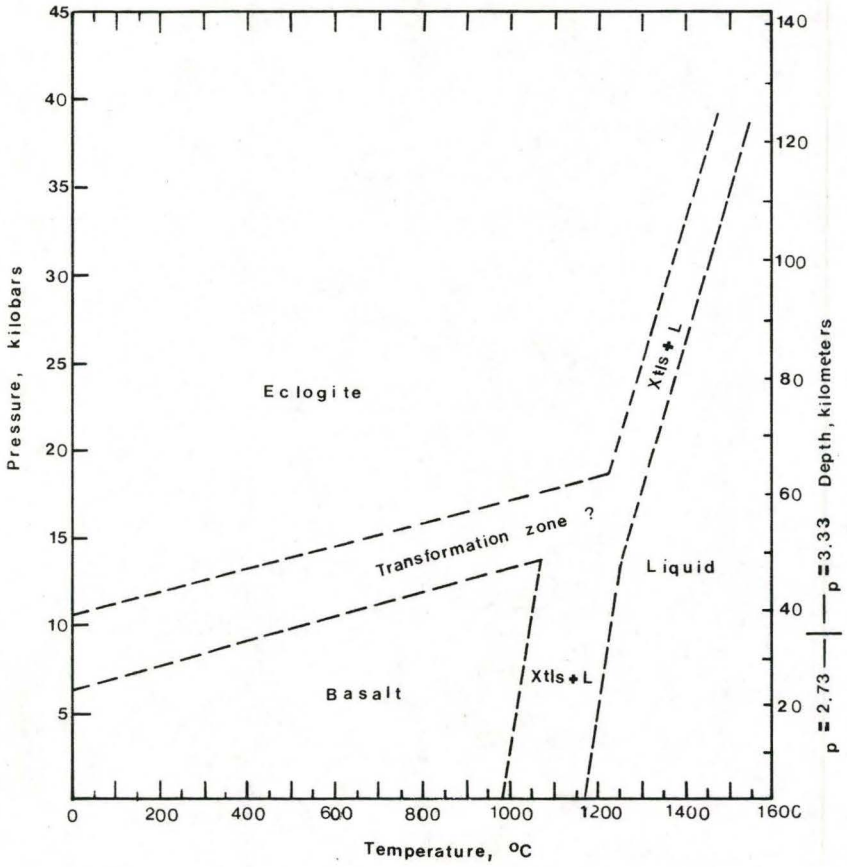

FIGURE 3.1 Pressure and temperature relations determined experimentally for a natural eclogite by Yoder and Tilley (1962). The question mark represents a pressure-temperature regime with complex transformations. Basalts are generally restricted to depths not exceeding 50 km.

material questions the validity of eclogites acting as source rocks for basaltic magma generation.

The mineralogy of garnet peridotite consists of olivine, orthopyroxene, clinopyroxene and garnet and the composition of these phases may be displayed in a tetrahedron (see figure 3.2). The composition of co-existing pyroxenes change as a function of temperature, and the solvus relating these changes (experimentally determined by Davis and Boyd, 1966) is relatively independent of pressure (Mysen, 1976). Another indirect pressure and temperature indicator is:

1) the alumina content of orthopyroxenes in the presence of garnet is a function of pressure (MacGregor, 1974). This relationship is also sensitive to temperature which must be estimated from the two pyroxene solvus.

Boyd and Nixon (1973) have used this indirect approach to determine the pressure and temperature regimes of pyroxenes found in nodules of garnet peridotite and kimberlite pipes. These nodules are found in alkali basalts and rarely in tholeiites but when present define the conditions under which they last equilibrated. The nodules indicate that they have equilibrated in a high pressure and temperature regime comparable to conditions in the upper mantle.

Ito and Kennedy (1967) have experimented on garnet lherzolites and spinel lherzolites at various temperature and pressure regimes. They found that a garnet lherzolite could generate an olivine-clinopyroxene-orthopyroxene-spinel assemblage

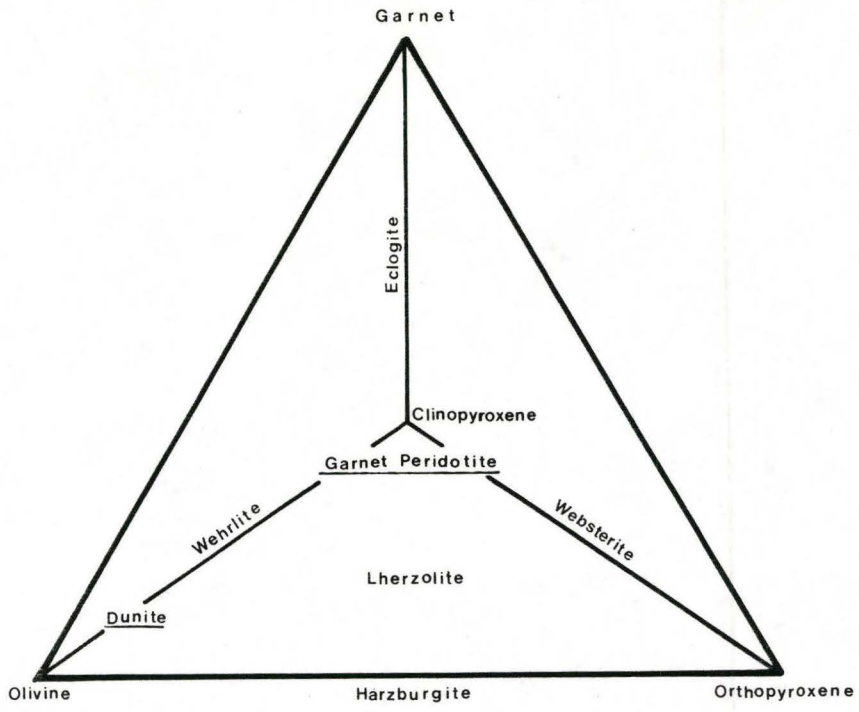

FIGURE 3.2 Nomenclature for rock assemblages in the garnet-clinopyroxene-orthopyroxene-olivine tetrahedron. Rock names that are underlined lie within the tetrahedron.

at pressures less than 20kb. The spinel lherzolite assemblage persisted at pressures less than 20kb but generated a garnet bearing assemblage at pressures exceeding 20kb. The prominent observation of these experiments is that neither assemblage produced a plagioclase reaction relation atl atm (see figure 3.3). The absence of plagioclase suggest that either:

1) these lherzolites do not have the appropriate composition to produce a basalt or,

2) the rock has been depleted of a basaltic component by partial melting and would therefore be considered a residuum.

This poses serious doubts as to whether a rock of this composition can yield a basalt, whose principal phase is plagioclase, if this type of source rock does not precipitate plagioclase at low pressures. Kushiro (1973) analyzed the glass produced by a sheared garnet lherzolite which was partially melted. He found that the results were compatible to a basalt in normative character although plagioclase was absent. It seems likely that partial melting of some undepleted peridotites are capable of yielding a liquid of basaltic composition if the crystals become isolated from the liquid. If this isolation of crystals and liquid is not achieved, then the peridotite will not necessarily precipitate plagioclase as a discreet phase, which presumably remains occult in the clinopyroxenes (Yoder and Tilley, 1962, Ito and Kennedy, 1967 and Kushiro, 1968).

Partial melting of garnet peridotite to produce a basaltic composition is supported by phase diagrams such as the

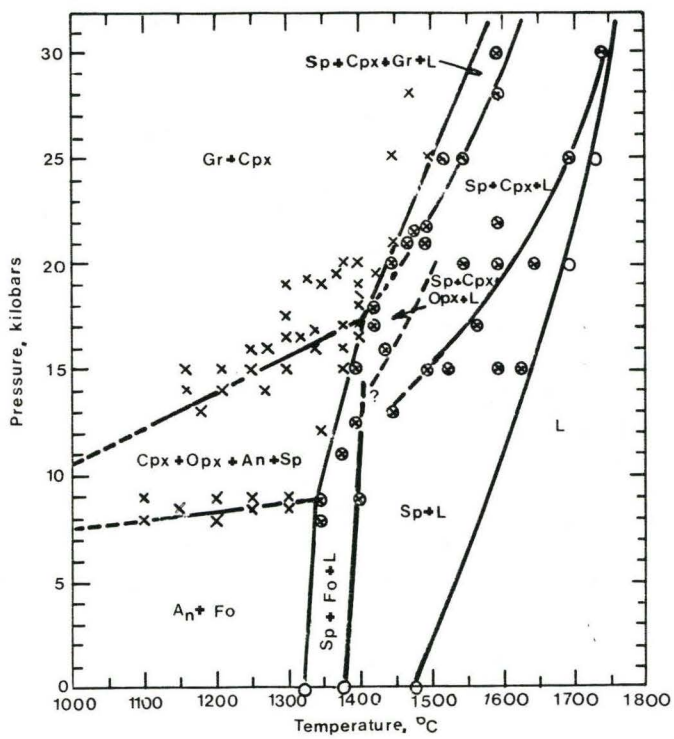

FIGURE 3.3 Pressure-temperature plane for the 1:1 composition (molecular ratio) of anorthite and forsterite. The symbols in the diagram indicate the conditions of the experiment: x=crstalline; ⊗=crystals + liquid; o=liquid; An=anorthite; Cpx=clinopyroxene; Fo=forsterite; L=liquid. From Kushiro and Yoder (1966).

forsterite-diopside-quartz (fo-di-SiO_2) system displayed in figure 3.4. The major features of this system are the large field of Fo_{ss} which overlaps most of the Di-En join which constitutes one edge of the plane of silica saturation and separates solid assemblages into two main groups:

1) those containing olivine and,

2) those containing silica

There is also the univariant curve R'QRM of liquids in equilibrium with olivine and pyroxene, and the univariant curve ESTM' of liquids in equilibrium with pyroxene and silica. The pigeonite field is relatively small but all liquids must reach and then depart the pigeonite field on fractional crystallization.

The basic principles of fractional crystallization within the fo-di-SiO_2 system for a bulk composition "X" (see figure 3.4), corresponding to a peridotite are discussed below. Initially, the liquid moves away from Fo_{ss}, then away from Pig across the Pig field until it readies the Di_{ss} boundary RT. The liquid is confined to this cotectic curve by the crystallization of Di_{ss} and Pig. When the liquid reaches T, reaction is prevented by fractionation and the liquid continues along the cotectic Tm with the crystallization of Di_{ss} and Tr. The liquid continues to the minimum m, where crystallization is complete.

All liquids produced by fractional crystallization with bulk compositions in the Fo_{ss} field arrive at the minimum m. The

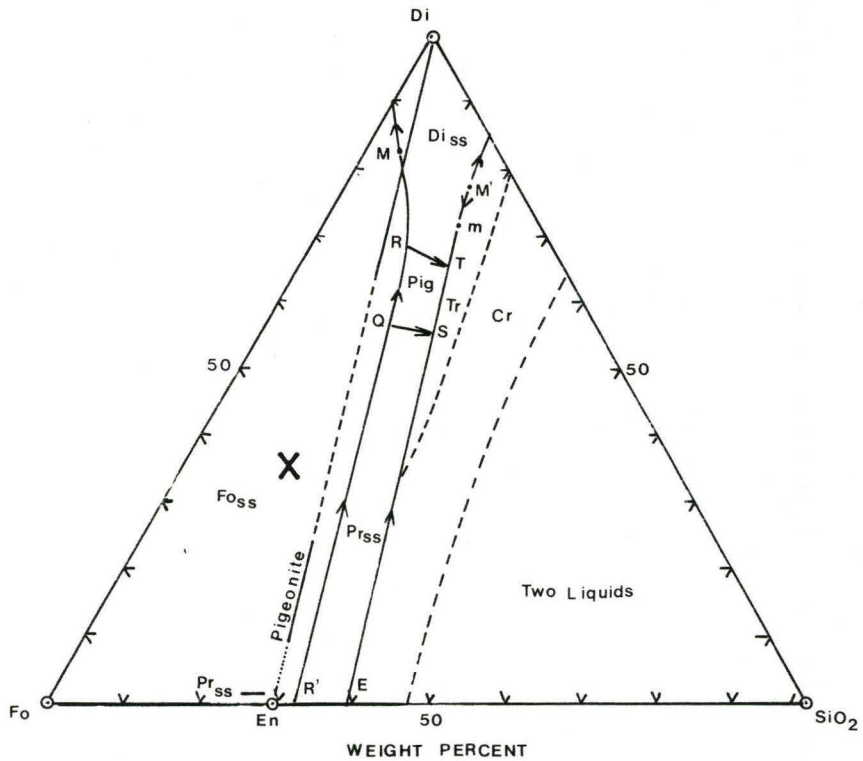

FIGURE 3.4 Phase equilibrium diagram of the system Fo-Di-SiO_2, revised by Kushiro(1972).

only variation of liquid paths is due to the initial Di:SiO_2 ratio. The failure of olivine and pyroxene to react with the liquid allows these phases to be preserved as isolated segregations and thereby increasing the amounts of SiO_2-producing liquids.

This is the basic pathway followed by a liquid which has been fractionally crystallized to produce a quartz bearing tholeiite. An important concept for compositions in the fo-di-en field is that they will produce initial liquids of basaltic compositions. The effect of hydrous conditions simply necessitates that there be more extensive melting to produce liquids of basaltic compositions than under anhydrous conditions.

The general consensus that garnet peridotite is a viable source rock for the generation of basaltic liquids is based on the following facts:

1) The occurrence of garnet peridotites are appropriate to deep seated environments.

2) Partial melting of garnet peridotites at high pressures have experimentally yielded liquids of a basaltic composition.

3) Garnet peridotites appear to satisfy density and seismic velocities encountered in the mantle.

4) The mineral assemblage of garnet peridotite is stable at high temperatures and pressures.

THE BASALT TETRAHEDRON: A MODEL FOR THE CLASSIFICATION OF BASALTS

The rate at which basaltic lava crystallizes greatly influences the nature of basaltic rock, causing a considerable degree of diversity. Rapidly quenched basaltic lava solidifies to glass, whereas a slowly cooled basaltic lava will crystallize a characteristic basaltic mineral assemblage. The mineralogy may be referred to in terms of minerals present (modal composition), and the chemistry of basalts may be expressed as either oxides or potential minerals which might form if the lava were to crystallize completely under ideal conditions.

Pyroxenes and plagioclase are the two most abundant minerals and may account for up to 80% of many basalts. The plagioclase is of an intermediate composition (An_{50}), generally andesine or labradorite. The pyroxene composition is commonly a more magnesian than ferrous rich variety $(Mg/(Mg+Fe)) > 0.5$, approximating diopside although it may range to subcalcic augite. A Ca-poor pyroxene (hypersthene) may or may not be present depending on the extent of silica saturation and is a critical mineral in the basaltic classification used to differentiate between tholeiitic and alkali basalts.

Olivine is another critical mineral in the classification and may be present instead of Ca-poor pyroxene in alkali basalts whereas, these two minerals co-exist in olivine tholeiites.

Nepheline and quartz are also used in the classification scheme due to their mutual incompatibility. Quartz and Ca-poor pyroxene may co-exist and olivine may also be present, but is

usually mantled by a more siliceous mineral. Olivine becomes unstable in the presence of excess silica due to the following reaction;

$$\underset{\text{Forsterite}}{Mg_2SiO_4} + \underset{\text{Quartz}}{2SiO_2} = \underset{\text{Enstatite}}{2MgSiO_3} \quad \ldots\ldots 4a$$

Nepheline is found in basalts which are undersaturated in silica; its presence is due to a deficency of silica. If silica were present, it would react with nepheline to form plagioclase;

$$\underset{\text{Nepheline}}{NaA/SiO_4} + \underset{\text{Quartz}}{2SiO_2} = \underset{\text{Albite}}{NaA/Si_3O_8} \quad \ldots\ldots 4b$$

This concept of silica undersaturation leads to a broad spectrum of basaltic rocks ranging from nepheline bearing (silica undersaturated) basalts to silica saturated tholeiites:

Basanite (nepheline bearing)	critically undersaturated
Alkali Basalt	critically undersaturated
Olivine Tholeiite	undersaturated
Hypersthene Basalt	saturated
Tholeiite (Quartz bearing)	oversaturated

The C.I.P.W. norm analysis is named after its inventors, Cross, Iddings, Pirsson and Washington, derives a series of potential minerals that could form if the rock crystallized completely under ideal conditions. The C.I.P.W. norm analysis is quite important when dealing with fine grained or glassy rocks whose actual mineralogy is often obscure or non-existent. The norm calculation also provides an important link between natural rocks and experimental systems based solely on chemistry. For a further discussion of C.I.P.W. norm calculations see Appendix 2B.

The basalt tetrahedron devised by Yoder and Tilley (1962) is a methodical approach used for classifying basaltic rocks based on their C.I.P.W. norms. The basalt tetrahedron (see figure 4.1) is a quaternary system using Fo-Di-Ne-SiO_2 as apices. Due to reaction 4a, plagioclase, which is represented by albite lies on the Ne-SiO_2 join. Diopside represents the pyroxenes at one apex while En lies between Fo and SiO_2 due to reaction 4b. The tetrahedron is divided by two planes;

1) the critical plane of silica undersaturation (Fo-Di-Ab) which separates the region of critically undersaturated rocks towards nepheline from regions of critically undersaturated and saturated regions towards quartz and,

2) the plane of silica saturation (En-Di-Ab) which separates the region of silica undersaturated rocks from the region of silica oversaturated rocks towards quartz.

The basalt tetrahedron allows the various types of basalts to be plotted according to their normative compositions. There are five basic groupings of basaltic rocks which occupy specific regions of the basalt tetrahedron (see figure 4.2) and have the following characteristics;

1) Tholeiite (silica oversaturated); Tholeiites have quartz and hypersthene in the norm and plot in the region to the right of the plane of silica saturation.

2) Hypersthene Basalt (saturated tholeiites); Hypersthene basalts have normative hypersthene and plot on the plane of

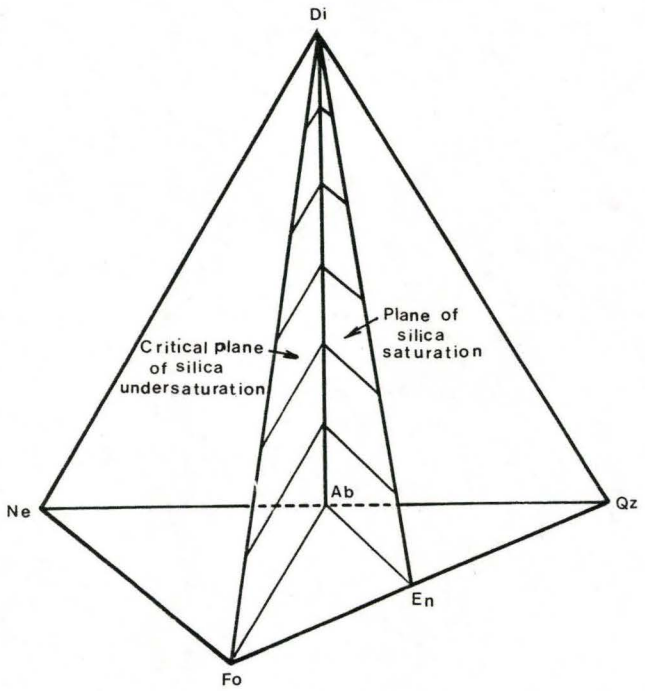

FIGURE 4.1 The fundamental basalt tetrahedron of Yoder and Tilley (1962), the system Di-Fo-Ne-Qz, showing the plane of silica undersaturation Di-Fo-Ab, and the plane of silica saturation Di-En-Ab. Although iron free, the system accounts for the major phases of basalts.

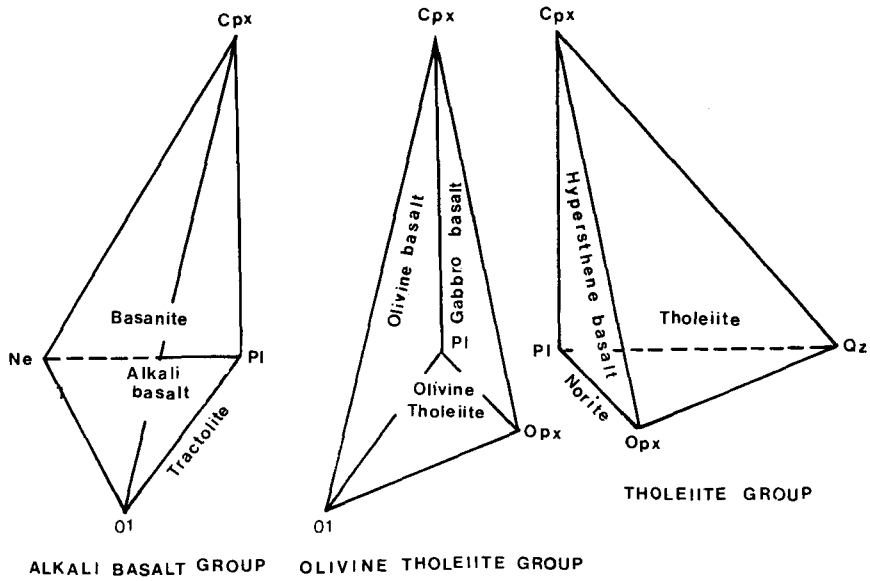

FIGURE 4.2 The basalt tetrahedron generalized to admit iron members of Di and Fo corners (i.e. olivine instead of the end member Fo, etc.), and An, and exploded to show nomenclature of major basalt types based on their normative composition.

silica saturation. These are rocks which have just enough SiO_2 to form hypersthene, but not enough for free quartz.

3) Olivine Tholeiite (silica undersaturated); Olivine tholeiites have hypersthene and olivine in the norm and plot in the region to the left of the plane of silica saturation.

4) Olivine Basalt (critically undersaturated in silica); Olivine basalts have olivine in the norm and plot on the plane of silica undersaturation. These rocks have just enough SiO_2 to form olivine but not enough to form hypersthene.

5) Alkali Basalt (critically undersaturated in silica); Alkali basalts have olivine and nepheline in the norm and plot in the region to the left of the critical plane of silica undersaturation.

PETROLOGY OF THE PARANÁ BASALTS

Based on the classification scheme adopted in the previous chapter, the Paraná basalts of the Misiones Province are all quartz tholeiites with hypersthene in the norm. Chemical analysis of these rocks and their associated C.I.P.W. norms appear in table 5.1 and it is quite apparent that these rocks are remarkably similar from a chemical viewpoint. The mineralogy of this suite of rocks is also relatively uniform throughout which is not surprising when considering the areal extent of some flood basalts (see table 2.1). This observation is quite apparent and easily verifiable by comparing individual modal compositions which appear in Appendix 3C. The only major variation relates to the amounts of volcanic glass relative to crystalline phases which is basically a function of the rate of cooling of the magma.

Plagioclase is the most abundant mineral (35-45%) in this suite of Paraná basalts and occurs as phenocrysts as well as a minor constituent of the glassy matrix. The plagioclase composition was determined by two independent methods;

1) Michel Lèvy tests

2) C.I.P.W. computation

Further discussion of the plagioclase composition is found later in this chapter and it is sufficient to say for the time being that the plagioclase had an intermediate composition ranging from andesine to labradorite.

TABLE 5.1
XRF MAJOR ELEMENT ANALYSES AND C.I.P.W. NORMS

	A-01	B-02	C-03	D-04	E-05	F-06
SiO_2	49.16	51.19	49.72	50.39	49.22	50.09
Al_2O_3	13.17	12.61	13.04	12.75	13.60	13.32
Fe_2O_3	7.791	9.761	10.469	9.506	9.841	9.759
FeO	7.70	6.14	5.74	6.40	4.89	5.11
MgO	5.70	4.72	4.10	5.14	6.12	5.36
CaO	9.72	8.77	8.24	8.91	10.22	9.21
Na_2O	2.01	2.04	2.13	1.81	2.15	1.86
K_2O	1.27	1.36	1.71	1.51	1.26	1.51
TiO_2	2.20	2.28	3.67	2.40	1.83	2.68
MnO	0.28	0.24	0.22	0.24	0.19	0.21
P_2O_5	0.26	0.29	0.41	0.34	0.23	0.41
total	99.261	99.401	99.449	99.396	99.551	99.519
Q	6.970	13.509	11.894	12.384	7.017	11.129
or	7.505	8.037	10.106	8.924	7.446	8.924
ab	17.008	17.262	18.024	15.316	18.193	15.739
an	23.164	21.235	20.971	22.207	23.738	23.538
total di	18.708	15.866	13.415	15.446	19.822	15.163
wo	9.754	8.510	7.195	8.258	10.632	8.133
en	6.766	7.356	6.219	6.979	9.190	7.030
fs	2.188	0.000	0.000	0.209	0.000	0.000
total hy	9.832	4.399	3.991	5.995	6.051	6.318
en	7.429	4.399	3.991	5.821	6.051	6.318
fs	2.403	0.000	0.000	0.174	0.000	0.000
mt	11.296	13.963	8.541	13.782	11.076	9.387
hm	0.000	0.130	4.551	0.000	2.202	3.285
il	4.178	4.330	6.970	4.558	3.476	5.090
ap	0.602	0.672	0.950	0.788	0.533	0.950

Explanation of column headings:
A-01 Quartz tholeiite near R. Garupa, 14km N. of Posadas.
B-02 Quartz tholeiite near Garruchos (Brazil side) on the Uruguay R.
C-03 Quartz tholeiite from bottom of San martin Cataratas.
D-04 Quartz tholeiite 5km S. of Alem on road to San Javier.
E-05 Quartz tholeiite 14km S. of Alem on road to San Javier.
F-06 Quartz tholeiite 30km S. of Iquazu Cataratas on road to Posadas.

TABLE 5.1 (cont'd)
XRF MAJOR ELEMENT ANALYSES AND C.I.P.W. NORMS

	G-07	H-08	I-09	J-10	K-11
SiO_2	51.97	49.01	49.09	49.48	49.99
Al_2O_3	12.61	13.35	13.65	13.78	12.53
Fe_2O_3	10.283	9.036	9.326	6.660	8.959
FeO	5.07	6.40	5.56	7.60	6.89
MgO	3.99	5.99	6.23	6.06	4.48
CaO	7.33	10.04	10.01	10.01	8.60
Na_2O	1.76	1.74	1.55	1.99	2.08
K_2O	2.21	1.22	1.34	1.16	1.84
TiO_2	3.48	2.08	2.12	2.04	3.22
MnO	0.17	0.16	0.25	0.23	0.26
P_2O_5	0.64	0.35	0.34	0.25	0.50
total	99.513	99.376	99.466	99.260	99.349
Q	16.060	9.101	9.727	6.097	11.277
or	13.061	7.210	7.919	6.855	10.874
ab	14.893	14.724	13.116	16.839	17.601
an	19.982	25.015	26.332	25.243	19.420
total di	9.502	17.665	16.433	18.299	15.618
wo	5.097	9.399	8.814	9.514	8.344
en	4.405	7.674	7.619	6.435	7.012
fs	0.000	0.592	0.000	2.350	0.262
total hy	5.531	7.802	7.896	11.819	4.300
en	5.531	7.243	7.896	8.657	4.145
fs	0.000	0.559	0.000	3.162	0.155
mt	6.809	13.101	12.590	9.657	12.989
hm	5.587	0.000	0.643	0.000	0.000
il	6.609	3.950	4.026	3.874	6.116
ap	1.483	0.811	0.788	0.579	1.158

Explanation of column headings:
G-07 Quartz tholeiite at bottom of Dos Hermanas (2 sisters) Falls
H-08 Quartz tholeiite 164km N. of Posadas on road to Iguazu.
I-09 Quartz tholeiite 209km N. of Posadas on road to Iguazu near Eldorado.
J-10 Quartz tholeiite 18km N. of Posadas on road to Iguazu.
K-11 Quartz tholeiite 120km N. of Posadas on road to Iquazu.

TABLE 5.1 (cont'd)
XRF MAJOR ELEMENT ANALYSES AND C.I.P.W. NORMS

	L-12	M-13	N-14	O-15	P-16
SiO_2	50.68	48.72	51.53	49.45	50.49
Al_2O_3	13.14	13.36	12.64	13.38	13.66
Fe_2O_3	7.468	13.220	8.391	11.341	8.372
FeO	7.83	3.65	6.76	3.60	5.60
MgO	4.70	6.13	4.67	6.99	5.92
CaO	9.29	8.82	8.66	8.08	9.91
Na_2O	2.03	1.90	1.98	1.53	1.93
K_2O	1.28	0.97	1.48	2.80	1.25
TiO_2	2.16	2.31	2.15	2.15	1.87
MnO	0.22	0.27	0.25	0.21	0.22
P_2O_5	0.27	0.31	0.29	0.32	0.26
total	99.248	99.660	99.341	99.644	99.482
Q	10.203	10.393	13.044	6.593	9.709
or	7.565	5.732	8.746	16.547	7.387
ab	17.178	16.078	16.754	12.947	16.331
an	22.963	23.062	21.232	21.373	24.919
total di	17.216	12.978	15.698	12.941	17.641
wo	8.920	6.961	8.283	6.942	9.415
en	5.847	6.017	6.350	6.000	7.859
fs	2.449	0.000	1.064	0.000	0.367
total hy	8.311	9.249	6.165	11.408	7.205
en	5.858	9.249	5.280	11.408	6.884
fs	2.453	0.000	0.885	0.000	0.321
mt	11.089	5.950	12.949	6.056	12.139
hm	0.000	9.116	0.000	6.957	0.000
il	4.102	4.387	4.083	4.083	3.552
ap	0.626	0.718	0.672	0.741	0.602

Explanation of Column headings:

L-12 Quartz tholeiite S. of Azara 1km over Corrientes-Missiones boundary in Corrientes.

M-13 Quartz tholeiite on Uruguay R. opposite Garruchos.

N-14 Quartz tholeiite on Garabi R. S.W. of Garruchos in the Corrientes Province.

O-15 Quartz tholeiite 179km N. of Posadas on road to Iguazu.

P-16 Quartz tholeiite 14km S. of Alem on road to San Javier.

TABLE 5.1 (cont'd)
XRF MAJOR ELEMENT ANALYSES AND C.I.P.W. NORMS

	Q-17	R-18	S-19	T-20	U-21	V-22
SiO_2	48.55	52.81	49.37	49.79	51.26	49.40
Al_2O_3	11.82	12.79	13.84	13.02	13.17	13.55
Fe_2O_3	13.990	7.721	8.915	12.109	11.165	6.933
FeO	4.58	7.91	5.47	4.18	3.07	7.78
MgO	7.00	4.07	6.31	5.46	4.76	5.65
CaO	8.17	8.06	9.80	8.68	8.85	9.89
Na_2O	2.07	1.65	2.08	2.23	2.38	2.01
K_2O	1.14	1.84	1.44	1.30	2.40	1.25
TiO_2	1.72	1.85	1.79	2.25	2.04	2.21
MnO	0.28	0.27	0.24	0.28	0.22	0.23
P_2O_5	0.24	0.27	0.22	0.29	0.38	0.36
total	99.560	99.241	99.476	99.589	99.695	99.263
Q	9.066	14.536	6.866	10.132	8.266	6.744
or	6.737	10.874	8.510	7.683	14.183	7.387
ab	17.516	13.962	17.601	18.870	20.139	17.008
an	19.595	22.059	24.176	21.678	18.166	24.260
total di	15.079	13.125	17.931	15.173	18.107	18.051
wo	8.088	6.750	9.607	8.139	9.712	9.376
en	6.991	4.108	8.236	7.034	8.395	6.289
fs	0.000	2.267	0.089	0.000	0.000	2.385
total hy	10.441	9.354	7.559	6.563	3.459	10.733
en	10.441	6.027	7.478	6.563	3.459	7.781
fs	0.000	3.327	0.081	0.000	0.000	2.952
mt	10.689	11.194	12.926	7.864	4.700	10.052
hm	6.618	0.000	0.000	6.685	7.924	0.000
il	3.267	3.514	3.400	4.273	3.874	4.197
ap	0.556	0.626	0.510	0.672	0.880	0.834

Explanation of column headings:
Q-17 Quartz tholeiite near Santa Ana on road from Posadas to Iguazu.
R-18 Quartz tholeiite 60km N. of Posadas near San Ignacio on road to Iguazu.
S-19 Quartz tholeiite 2km S. of Azara.
T-20 Quartz tholeiite on the Uruguay R. near Garruchos.
U-21 Quartz tholeiite 185km N. of Posadas on road to Iguazu.
V-22 Quartz tholeiite from a small quarry 3km from Iguazu Falls.

TABLE 5.1 (cont'd)
XRF MAJOR ELEMENT ANALYSES AND C.I.P.W. NORMS

	W-23	X-24	Y-25	Z-26	MEAN
SiO_2	49.88	51.04	48.50	49.47	50.01
Al_2O_3	13.87	13.64	13.50	13.57	13.21
Fe_2O_3	9.439	13.278	10.513	8.653	9.75
FeO	5.11	2.62	4.76	6.22	5.64
MgO	5.94	3.99	5.77	5.37	5.41
CaO	10.47	8.68	9.82	9.81	9.16
Na_2O	1.76	2.13	1.70	2.12	1.95
K_2O	0.72	1.50	1.82	1.54	1.50
TiO_2	1.83	2.29	2.54	2.13	2.28
MnO	0.24	0.25	0.24	0.23	0.23
P_2O_5	0.25	0.33	0.39	0.29	0.33
total	99.509	99.748	99.553	99.403	99.470
Q	11.159	13.110	7.927	7.639	-
or	4.255	8.865	10.756	9.101	-
ab	14.893	18.024	14.385	17.939	-
an	27.821	23.228	23.831	22.964	-
total di	17.508	13.763	17.392	18.706	-
wo	9.391	7.382	9.392	9.943	-
en	8.117	6.381	8.063	8.051	-
fs	0.000	0.000	0.000	0.713	-
total hy	6.676	3.556	6.306	5.793	-
en	6.676	3.556	6.306	5.332	-
fs	0.000	0.000	0.000	0.471	-
mt	11.948	2.623	8.762	12.546	-
hm	1.199	11.469	4.470	0.000	-
il	3.476	4.349	4.824	4.045	-
ap	0.579	0.765	0.904	0.672	-

Explanation of Column headings:
W-23 Quartz tholeiite 9km S. of Alem on road to San Javier.
X-24 Quartz tholeiite near General Güemes, 20km E. of San Jose.
Y-25 Quartz tholeiite 160km N. of Posadas on road to Iguazu.
Z-26 Quartz tholeiite 170km N. of Posadas on road to Iguazu.
MEAN This is the arithmetic mean of the samples analyzed.

Some larger plagioclase phenocrysts with dimensions approaching 2.0x0.4mm were observed but these tend to be relatively rare. More common are the elongated, subhedral laths with average dimensions of 0.4x0.1mm and equidimensional crystals (0.2x0.2mm).

Albite and combined albite-carlsbad twins were the most frequently observed although there were infrequent crystals which displayed pericline twins. Although the types of twinning observed was quite consistent, there was a considerable variety in the nature of the twinning. Plagioclase crystals ranged from crystals with crisp, well-defined twins to clouded crystals with gradational boundaries between twins. These two distinctive modes of twinning were commonly observed co-existing together in many of the thin sections and there was no evidence to suggest that clouded plagioclase crystals were preferred to plagioclase crystals with well-defined twins in certain thin sections and vice versa.

Many of the plagioclase laths when in contact with volcanic glass displayed corroded boundaries and battlement ends signifying that there has been a volcanic glass-plagioclase interaction. These plagioclase crystals were commonly clouded and this may be attributed to their association with the volcanic glass. Crystals that were relatively isolated from volcanic glass displayed well-defined twins and this association with

volcanic glass (or lack of) appears to be a controlling factor in determining the nature of the twinning in plagioclase crystals.

The process producing clouded crystals may be attributed to inclusions of finely disseminated dark particles (probably an Fe-oxide) derived from:

1) the exsolution of Fe^{+3} which substitutes for Al in the feldspar structure,

2) incorporation of Fe into the crystal subsequent to its crystallization or,

3) low grade thermal metamorphism.

Further intensification of clouding may be attributed to continuing diffusion of Fe into the crystal after it crystallized. The close association of clouded plagioclase laths with volcanic glass suggest that the volcanic glass is acting as a source material providing the Fe to be incorporated within the plagioclase crystals. To support this hypothesis is the observation that the volcanic glass often contained considerable amounts of opaque Fe-oxides and a green iron silicate (chlorite?) which may act as source minerals for the exsolution and diffusion of Fe^{+3} into the plagioclase crystals.

Plagioclase laths are often crossfractured which have subsequently been infilled by volcanic glass or epidote (?) (see photomicrograph 5.1a). The formation of epidote is favoured by shearing stress and low temperatures but it will also crystallize in the absence of stress as a product of the hydrothermal alteration (saussuritization) of plagioclase. Volatile analysis

for the identification of H_2O^+, H_2O^-, CO_2, F and Cl were not conducted and may be incorporated in further research projects. Of these volatiles, H_2O is usually the most abundant with variable amounts of the other volatiles. Volatiles may be concentrated in a residual vapour phase which interacts with original magmatic minerals forming new minerals by a process known as deuteric alteration. Epidote is a common product of deuteric alteration and is often associated with plagioclase by the following reaction:

$$3CaAl_2Si_2O_8 + H_2O + CaCO_3 = 2Ca_2Al_3Si_3O_{12}(OH) + CO_2$$
Anorthite Calcite Epidote

The elongated plagioclase laths were commonly observed forming wedge shaped interstices. These interstices were commonly filled with either:

1) a combination of an unidentifiable, extremely fine grained crystalline aggregate with volcanic glass forming an intersertal texture (see photomicrograph 5.2b) or,

2) crystals of other minerals (commonly pyroxene) forming an intergranular texture.

The intersertal texture was more common than the intergranular texture due to the abundance of volcanic glass found in these thin sections. There was often a transitional type of texture between these two 'end-members' which filled the interstices with microphenocrysts set in a glassy matrix.

Another common textural feature displayed by the plagioclase laths is a subophitic texture whereby the laths are partially enclosed in pyroxene phenocrysts (see photomicrograph 5.3c). The

significance of this texture is that it indicates that the two constituents involved have crystallized simultaneously.

Very rarely (only displayed in samples G-07 and J-10) were the plagioclase laths aligned subparallel to the direction of flow of the magma, resulting in a trachytic texture. This was however, a discontinuous feature even in these slides.

Zoning of plagioclase phenocrysts was quite common in the majority of thin sections. The zoned phenocrysts (see photomicrograph 5.4d) usually had a wide central core of Ca-rich plagioclase which is surrounded by narrower zones of Na-rich plagioclase. The wide Ca-rich core signifies that they were formed during periods of slow crystallization (relative to outer narrow zones) before the final consolidation of the magma.

This zoning phenomenon may be accounted for by assuming fractional crystallization was a viable mechanism operating during the crystallization of these rocks.

The system albite ($NaAlSi_3O_8$) - anorthite ($CaAl_2Si_2O_6$) is a binary system with continuous and complete solid solution between the two end members.* Albite is related to anorthite by the exchange:

$$NaSi \leftrightharpoons CaAl$$

Due to this exchange reaction, albite is more siliceous and less aluminous and contains an alkali cation instead of an alkaline earth cation.

* This is strictly true at high temperatues and low to moderate pressures. At metamorphic temperatures and pressure the system may deviate from these conditions.

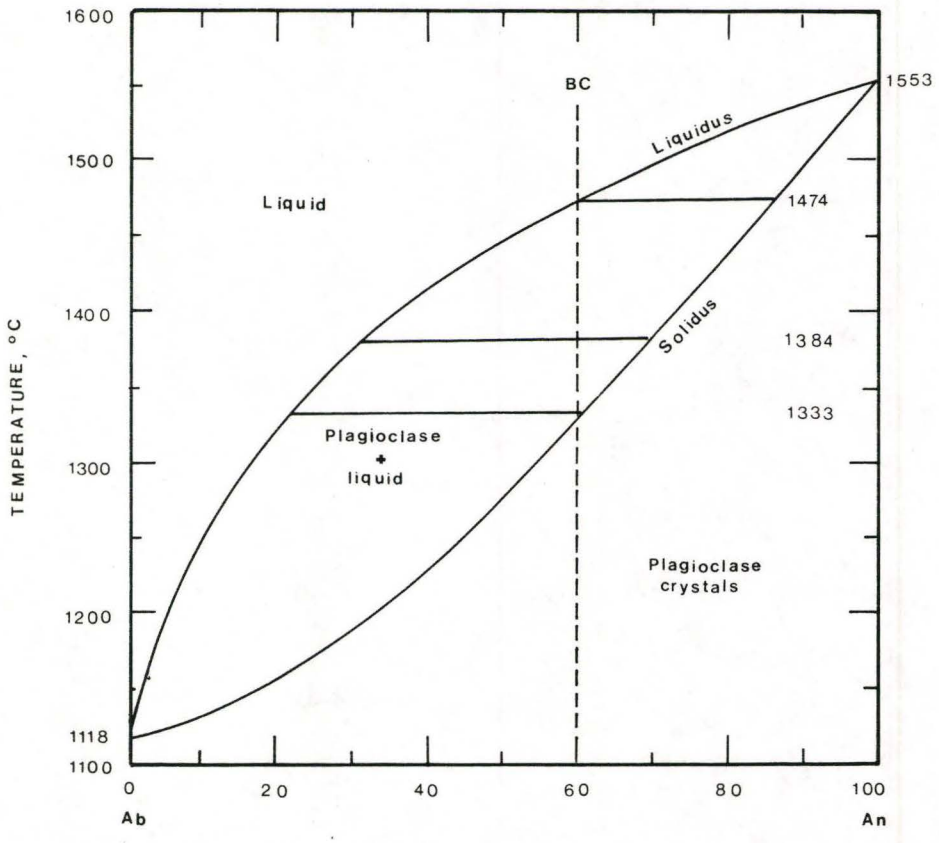

FIGURE 5.1 Crsystallization in the system An-Ab.

The plagioclase system (see figure 5.1) illustrates the course of crystallization for a bulk composition $An_{60}Ab_{40}$. For this composition, crystallization is intitiated at the intersection of the liquidus at 1474°C. The initial crystals that form have a composition of An_{86} and are more calcic than the liquid at this temperature. This process continues with decreasing temperature and both the liquidus and crystal composition become more sodic. In order for the crystals to maintain equilibrium with the liquid as the crystals become more Ab-rich, the early formed calcic crystals must react with the liquid to change to more sodic crystals. This condition demands a slow gradual decrease in temperature to necessitate the intracrystalline diffusion of $Al \rightleftharpoons Si$ and $Na \rightleftharpoons Ca$. This reaction of crystals with liquid with gradual decreases of temperature is known as equilibrium crystallization.

Equilibrium crystallization is not a viable mechanism for the production of zoned plagioclase crystals that were so common in these quartz tholeiites. The production of zoned plagioclase crystals requires the failure of reaction between liquids and crystals. Inhibiting this diffusion process may be accomplished by more rapid decreases in temperature (or the physical removal of crystals by floating or sinking) leading to fractional crystallization.

Fractionally crystallizing a bulk composition $An_{60}Ab_{40}$ begins again at 1474°C with the separation of crystals with the composition An_{86}. These crystals do not react with the liquid

and with decreasing temperature the following crystals are slightly more sodic than the earlier formed crystals. This process is repeated with decreasing temperature and progressively more sodic crystals are formed.

The isolation of earlier formed crystals prevents the exchange reaction $NaSi \leftrightharpoons CaAl$ from taking place. This allows the conservation of Na and Si in the liquid and depletion of Ca and Al in the liquid. Thus, fractional crystallization is a viable mechanism which produces a range of liquid compositions all the way from the initial composition of the melt to pure albite which is distinctly different from equilibrium crystallization.

The plagioclase crystal composition was determined by Michel Lèvy tests and was also computed by the C.I.P.W. program. The Michel Lèvy test produced results that ranged from An_{46} to An_{54}. The C.I.P.W. albite ratio (ab/(ab+an)) produced values slightly more sodic than the Michel Lèvy test and ranged from An_{33} to An_{53} with an average for the suite of An_{42} (see table 5.1 and appendix 3C).

One possible solution for the discrepancy between the Michel Lèvy and C.I.P.W. results may be related to the process of fractional crystallization. Plagioclase crystals used to determine the An content by Michel Lèvy tests were the larger phenocrysts, whereas the smaller, late stage plagioclase laths incorporated into the glassy groundmass were ignored. Thus, if fractional crystallization was a viable operating mechanism, it can be assumed that the late stage plagioclase laths found

interstitially and incorporated into the glassy groundmass were albite rich. The calculated C.I.P.W. albite ratio assumes that the rock has crystallized completely under ideal conditions and would take into account plagioclase crystals formed both early and late in the crystallization sequence and thus explains the sodic enriched values relative to the Michel Lèvy results.

Pyroxenes typically account for 15-25% of most thin sections observed in this suite of rocks. Clinopyroxenes are characteristically much more abundant than the orthopyroxenes and the clinopyroxene/orthopyroxene ratio may approach 5 or 6. This is attributed to the fact that clinopyroxenes were characteristically found as phenocrysts, whereas the orthopyroxenes were more commonly found as constituents of the glassy groundmass. Phenocrysts of orthopyroxenes were rare, but when present often displayed good crystal form.

The differentiation between orthopyroxenes and clinopyroxenes in thin section was readily made based on their different interference colours. However, the type of clinopyroxene (pigeonite or augite, etc.) or orthopyroxene present was complicated due to the lack of obtainable optic figures and $2V^S$. This is attributed to the fact that the majority of the pyroxene crystals were relatively fine grained. This will cause optic figures to be influenced by neighboring crystals and will render results that may be misleading or meaningless. Further analysis by more sophisticated methods

(electron microprobe) would be extremely beneficial in aiding pyroxene identification.

The pyroxenes were identified as best as possible using the parameters of colour in thin section, refractive index, cleavage, extinction angles, interference colours, birefringence and habit. The orthopyroxene, hypersthene was usually a pale pink or green in thin section and commonly displayed a faint pleochroism. Hypersthene was easily differentiated from the clinopyroxenes by its first order yellow interference colour.

The clinopyroxene identification was more difficult due to the similar properties of many of the clinopyroxenes. Clinopyroxene identification is favoured by obtaining numerous optic figures but in this suite of rocks, optic figures were virtually non-existent. The clinopyroxene, identified as augite, commonly displayed a flesh colour in thin section. Some augite crystals were observed displaying a violet colour in thin section which is a characteristic feature of Ti-bearing augites. Another common feature displayed by many of the augite crystals was colour zoning.

Augite in this suite is encountered as anhedral to subhedral phenocrysts that are easily differentiated from the other minerals observed in these thin sections by its higher interference colours (low third order). Some augite phenocrysts were relatively large (with dimensions approaching 0.5x0.5mm) compared to other phenocrysts of plagioclase and hypersthene.

These large phenocrysts often displayed a subophitic or ophitic texture which totally enclosed smaller plagioclase laths.

Some of these larger augite phenocrysts were not true phenocrysts, but occurred as aggregates of smaller augite phenocrysts. This amalgamation of augite pheoncrysts was quite common in these thin sections and formed a glomeroporphyritic texture. This textural feature is a product of synneusis which is a process whereby augite phenocrysts drift together in the melt and become mutually attached.

Augite phenocrysts were the most common form, but there were other minor modes of occurrence. These included:

1) microphenocrysts of augite incorporated into the glassy groundmass and,

2) anhedral augite crystals occupying wedge shaped interstices formed by plagioclase laths.

Augite crystals characteristically displayed very little evidence of alteration. This was also apparent when augite crystals were confined to the groundmass unlike other constituents which were highly altered. Some phenocrysts that were fractured had subsequently been infilled with volcanic glass and/or hematite. Augite crystals that were hematite stained commonly contained ferrosillite in their normative composition. This association of augite crystals with hematite staining may be attributed to:

1) the diffusion of Fe from the crystal structure or,

2) the interaction of Fe-rich fluids (or a residual vapour phase) with the augite crystals.

Glomeroporphyritic aggregates of augite phenocrysts commonly contained volcanic glass between the individual phenocrysts that accentuated crystal boundaries. This phenomenon is probably not a product of alteration but a result of the trapping of the melt when the augite phenocrysts amalgamated.

Augite phenocrysts often displayed colour zoning and a faint pleochroism when viewed in plane polarised light. Cores of augite crystals commonly had a faint purple tint which increased in intensity towards the margins of the crystal. This may be due to compositional changes within the crystal which is a common feature of Ti-bearing augite.

In the glassy groundmass of many thin sections was a clinopyroxene which displayed lower interference colours than augite. This is most likely the Ca-poor pyroxene pigeonite. Pigeonite was never observed as phenocrysts and even its presence in the glassy groundmass was minimal. Uninverted pigeonite occurs only in rapidly chilled rocks and is, therefore, restricted to lavas formed by rapid crystallization. Some samples displayed inverted pigeonite which was identified by the presence of augite lamallae located along the (001) plane of the original pigeonite and, in twinned crystals by the herring-bone pattern of the lamallae (see photomicrograph 5.5e).

The plane $CaSiO_3$(Wo)-$MgSiO_3$(En) - $FeSiO_3$ (Fs), contains the pyroxene quadrilateral which displays the major rock forming pyroxenes contained in basaltic rocks (see figure 5.2). Augite, a Ca-rich pyroxene and pigeonite (Ca-poor) commonly form

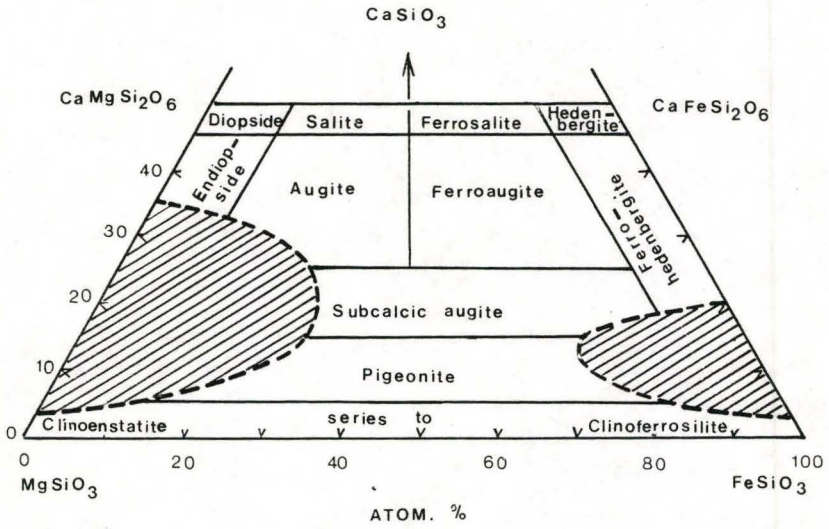

FIGURE 5.2 Terminology of clinopyroxene in the system $CaMgSi_2O_6$-$CaFeSi_2O_6$-$MgSiO_3$-$FeSiO_3$. The shaded areas represent areas of immiscibility and lacking naturally occurring examples.

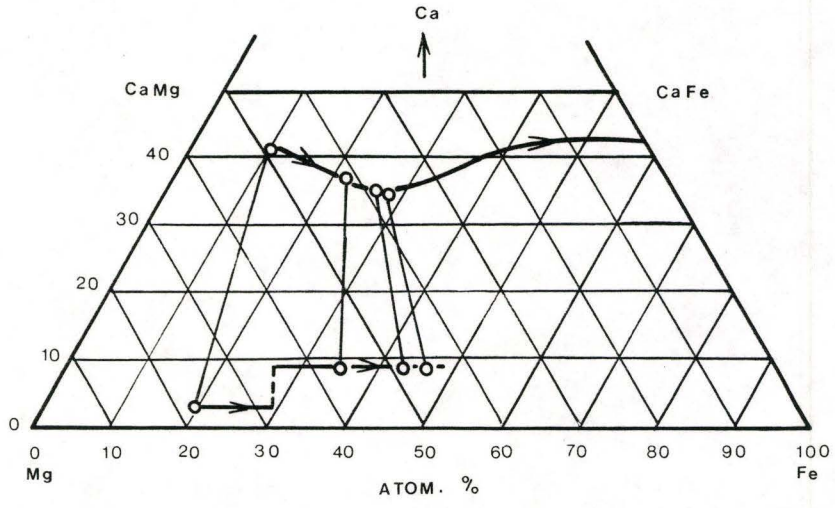

FIGURE 5.3 Crstallisation trends and coexisting pyroxene pairs (tied circles).

early in the fractional crystallization sequence of many tholeiitic magmas (see figure 5.3). During the initial stages of crystallization, Ca rich pyroxenes typically have a composition approximating $Ca_{45}Mg_{45}Fe_{10}$ and the Ca-poor phase has a composition approximating $Ca_4Mg_{77}Fe_{19}$. Continued differentiation causes both pyroxenes to become Fe-enriched. This trend of Fe-enrichment in Ca-rich pyroxenes may continue to produce a Ca-rich ferroaugite, but the Ca-poor pyroxene ceases to exist in cases of extreme fractionation and generally does not become more Fe-rich than $Ca_{10}Mg_{45}Fe_{45}$. The limit of the composition field in which two pyroxene phases crystallize together is termed the two pyroxene field boundary. Beyond the two pyroxene field boundary, pigeonite inverts to orthorhombic symmetry and this causes the exsolution of $CaSiO_3$ as augite lamallae, forming the herring-bone texture observed in these thin sections.

Hypersthene in the Paraná basalts is rarely found as phenocrysts and it is more commonly a constituent of the glassy groundmass. Hypersthene was much less abundant than the clinopyroxenes and typically accounted for 2-5% of most thin sections. This abundance does not take into account hypersthene incorporated into the glassy groundmass and is the abundance of hypersthene phenocrysts only.

Hypersthene phenocrysts were typically anhedral to subhedral and had dimensions of approximately 0.4x0.4mm. Many of these phenocrysts displayed a subophitic to ophitic texture with the

plagioclase laths. Alteration was minimal with only minor hematite staining in thin sections where hypersthene contained a ferrosillite component in its normative composition. The processes accounting for this phenomenon are probably similar to those discussed earlier regarding the association of hematite with augite. Alteration was more pronounced in hypersthene microphenocrysts incorporated into the glassy groundmass where volcanic glass-hypersthene interaction has resulted in anhedral crystals.

Opaque Fe-oxides were quite common in this suite. The differentiation between magnetite and ilmenite was based on ilmenites skeletal nature but this is not always possible. This distinction was virtually impossible when the opaque Fe-oxides were confined to the glassy groundmass due to extensive interaction with the volcanic glass. For the remainder of this report, ilmenite and magnetite will be referred to as opaque Fe-oxides.

Opaque Fe-oxides were common as xenoblasts as well as constituents of the glassy groundmass. This is not surprising due to the fact that this is quite a Fe-rich suite (see chapter six). The xenoblasts were typically anhedral although some displayed a slightly more developed crystal shape. The size of the xenoblasts showed a considerable range with some having dimensions approaching 0.5x0.5mm. These large xenoblasts, however, were considerably rare and the majority of opaque Fe-oxides were much smaller and found interstitially.

Opaque Fe-oxides were a common constituent of the glassy groundmass. They were typically found disseminated throughout the glassy groundmass as fine grains in various stages of alteration. The exact boundaries were often hard to discern as alteration has produced gradational boundaries between the opaque Fe-oxides and iddingsite (iddingsite is discussed later in this Chapter).

Although SiO_2 was the most abundant oxide, quartz was only a minor constituent in this suite of rocks. The majority of SiO_2 available to form quartz has probably been incorporated into the siliceous residue forming the glassy groundmass. This hypothesis is supported by the presence of quartz microphenocrysts in the glassy groundmass and the large discrepancy in the abundance of quartz reported in the C.I.P.W. norm and the actual modal percentages observed. Quartz phenocrysts were typically small and ranged from anhedral to subhedral. Quartz was more commonly found as a late stage mineral that had two distinctive modes of occurrence:

1) as microcrystalline aggregates lining vesicles and amygdules. The microcrystalline nature of the quartz infers that the magma was probably rapidly quenched and,

2) as subhedral crystals infilling vesicles. This form of quartz was likely formed during periods of more gradual decreases in temperature.

The groundmass and volcanic glass components of the Paraná basalts are quite variable in both their nature and abundances.

It is not always possible to identify the groundmass, volcanic glass and their associated alteration products as mineral species because in most cases, colour in thin section, habit and interference colours are the only observable features. Even these characteristics are often obliterated due to the amorphous nature of the groundmass which has a two fold effect:

1) the groundmass appears as an extremely fine grained microcrystalline matrix making it virtually impossible using petrographic technique available to positively identify mineral species and,

2) interaction between microphenocrysts enclosed within the crystalline matrix tend to be altered to some extent which also increases the difficulty of positively identifying mineral species.

Although positive identification may not always be possible, the glassy groundmass displays certain characteristics which persist in most of these samples.

The determination of the chemical composition of the glassy groundmass cannot be accurately estimated by the techniques available in this report. However, a crude estimate can be made based on the discrepancies in the C.I.P.W. normative minerals expected if the rock has crystallized completely under ideal conditions and the observed modal percentages. Quartz, hematite, magnetite, orthoclase, ilmenite and apatite were generally found in greater abundances in the C.I.P.W. norm than in their corresponding thin sections. This would suggest that these

minerals, or their components are concentrated in the glassy groundmass.

There was basically two distinctive modes of late stage aggregates:

1) a reddish-brown amorphous substance that will be referred to as iddingsite and,

2) a green Fe-silicate that will be referred to as chlorite. Positive identification of these substances requires further research and more sophisticated techniques such as electron microprobe analysis. Wilshire (1958) has described iddingsite as a mixture of Fe-oxides in various stages of oxidation and hydration and has proposed a tentative formula of $MgO\text{-}Fe_2O_3\text{-}3SiO_2\text{-}4H_2O$. The green Fe-silicate referred to as chlorite belongs to a group of minerals (bowlingtonite, nontronite, saponite and vermiculite) Wilshire classified as members of the serpentine group.

Iddingsite is a deuteric substance formed in the presence of volatiles, vapour phases, elevated temperatures and in oxidizing conditions. Volatile rich fluids producing late stage alteration of ferromagnesian minerals leach MgO from these minerals which subsequently becomes incorporated into the melt. These fluids generally contain a high concentration of Fe and it is not surprising that the volcanic glass is relatively enriched in these two elements compared to the crystalline phases. This Fe-enrichment of the late stage quench products also accounts for the discrepancy between C.I.P.W. normative magnetite (and other

opaque Fe-oxides) being considerably more abundant than the magnetite actually observed in the corresponding thin section.

This process of late stage fluids leaching the principal oxides out of pre-existing minerals appears to have been a viable operating mechanism in many of these samples. This process would be most efficient at grain boundaries where the fluids interact with the minerals (see photomicrograph 5.6f). Many phenocrysts and microphenocrysts enclosed within iddingsite displayed altered boundaries but their cores are relatively unaltered. This was quite apparent in some of the larger phenocrysts which displayed thin outer zones that were highly altered due to this interaction. Microphenocrysts were often totally altered due to their larger surface area/volume ratios which allows more complete interaction with the melt. Chlorite was generally absent as an alteration product of (micro)phenocrysts. When chlorite was observed as an alteration product, it was preferentially associated with the pyroxenes. I was unable to find a reaction to account for this but it must liberate CaO because it is not incorporated into the chlorite structure.

Volcanic glass is a metastable substance and is crystallized (or devitrified) in most of the samples. The presence of water is a very effective agent in increasing the rate of devitrification of volcanic glass. Perlite, a hydrated glass (commonly containing 2-5% H_2O) often displayed arcuate cracks due to the volume change produced by hydration. Perlitic volcanic glass, when present in these thin sections appeared as

isolated, deep reddish-brown anhedral 'crystals' infilling interstices between minerals. Perlitic volcanic glass was typically less abundant than other forms observed throughout the suite.

The most common form of glassy groundmass consisted of an amorphous, dark reddish-brown microcrystalline matrix of iddingsite enclosing numerous microphenocrysts (see photomicrograph 5.7g). These microphenocrysts generally account for only a small proportion of the glassy-groundmass and are commonly plagioclase, quartz, opaque Fe-oxides, orthoclase and hypersthene. The plagioclase laths were the most abundant microphenocrysts enclosed within the glassy groundmass and were probably a very sodic rich variety due to fractional crystallization.

The volcanic glass commonly displayed characteristic growth patterns that were quite common in the majority of the observed thin sections. Spherulitic growth patterns were commonly observed (see photomicrograph 5.8h) which is due to growth originating at a point source which radiates outwards. Axiolitic growth patterns (see photomicrograph 5.9i), which is due to growth originating from a line source was commonly displayed by chlorite. A rare textural feature displayed by the volcanic glass was banding due to the flowage of the magma (see photomicrograph 5.10j).

Chlorite was commonly found associated with the glassy groundmass and lining amygdules. When chlorite was contained

within the iddingsite, crystals were not encountered, although some green, fibrous chlorite was observed. The presence of chlorite within the groundmass was easily detected due to its prominent green colouration. The chlorite did not appear to be an alteration product of the glassy matrix and is probably a result of late stage crystallization from a residual liquid. Chlorite is commonly found as a product of hydrothermal alteration or as a deuteric mineral and its occurrence in these quartz tholeiites may be due to late stage interaction of a residual vapour phase with pre-existing ferromagnesian minerals.

Chlorite in these samples did not generally appear as a replacement product of pre-existing minerals. Based on chlorites shape and orientation, it appears that it has been precipitated from a liquid phase that has subsequently been rapidly quenched. The formation of chlorite from a rapidly quenched liquid has been reported by Schrairer and Yoder (1964) in their studies on the system Mg-cordierite-H_2O. Chlorite that was associated with iddingsite may be explained by its crystallization from a glass that followed the initial intrusion quench.

Chlorite was often found lining vesicles and amygdules that were subsequently infilled by quartz and plagioclase (see photomicrograph 5.11k). Chlorite was either fibrous or amorphous and its structure is a function of the rate of decrease in temperature. Rapid decreases in temperature would produce disordered structures (amorphous) whereas more gradual decreases would allow the development of more ordered crystals.

Fibrous chlorite lining vesicles often displayed variations in its colour. Chlorite had a deeper, more intense green colouration at the margins of the vesicle but is colour changed to a much paler green as the fibres protruded into the vesicle. This reflects a higher Fe^{+2}/Fe^{+3} ratio at the margins which progressively decreased due to the decreasing partial pressure of oxygen with continued crystallization. This type of chlorite is definitely not an alteration product of pre-existing minerals but is a genetic product of deuteric alteration.

Iddingsite was more abundant than chlorite in the vast majority of these samples but their relative abundances are quite variable. Green chlorite was often associated with iddingsite in various proportions in many of the specimens. The abundances of iddingsite and chlorite appears to be related to the relative abundances of FeO and Fe_2O_3. Samples with high FeO/Fe_2O_3 ratios (>0.75) generally corresponded to higher chlorite contents whereas lower FeO/Fe_2O_3 ratios correspond to samples with glassy groundmasses dominated by iddingsite.

The only major petrographic variation noted during the examination of these thin sections was the relationship between the reddish-brown and the green components of the glassy groundmass. This relationship is essentially due to the various oxidation states of Fe. Products of alteration in this suite were often observed with iddingsite (and minor chlorite) mixed with Fe-oxides in various states of oxidation and hydration. The

nature of the alteration products and the Fe-oxides are a function of:

1) the composition of the original mineral,

2) the composition of the late stage fluid and,

3) most importantly is the rate of cooling during the alteration process.

Photomicrograph 5.1a Cross fractured plagioclase crystal which has subsequently been infilled by volcanic glass and epidote. Also notice altered plagioclase margins (Q-17, magnified 160 times).

Photomicrograph 5.2b Intersertal texture between plagiclase laths. Note the spherulites in the glassy groundmass (L-12, magnified 160 times).

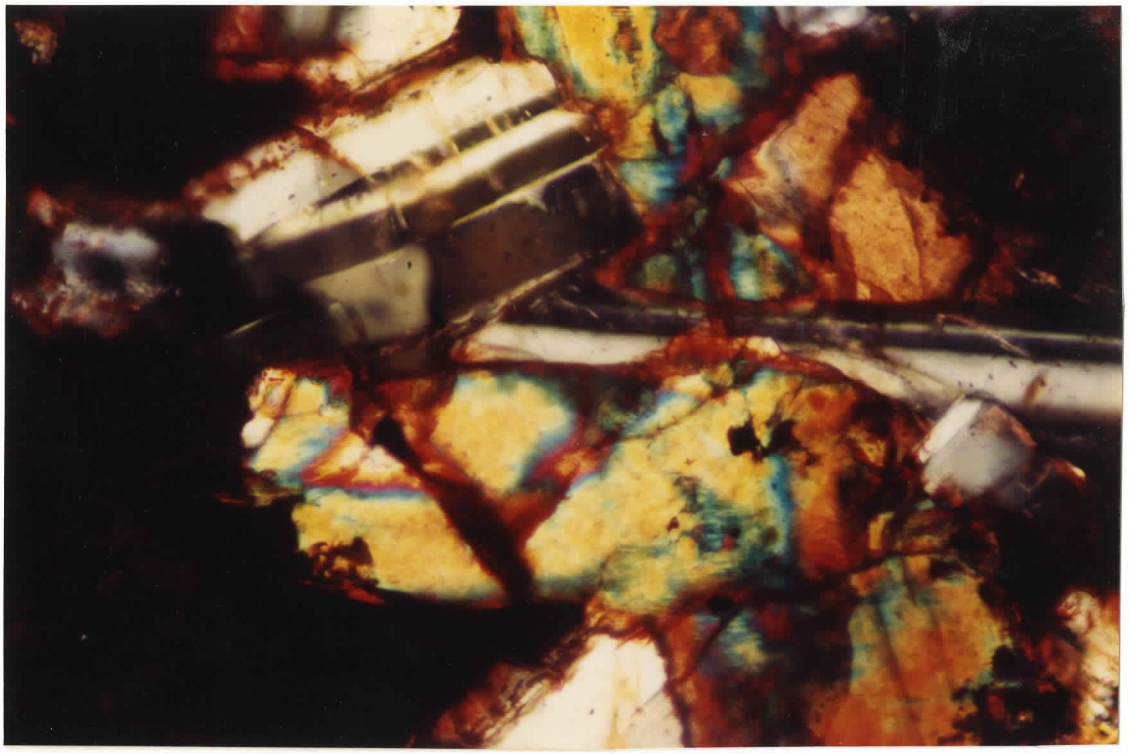

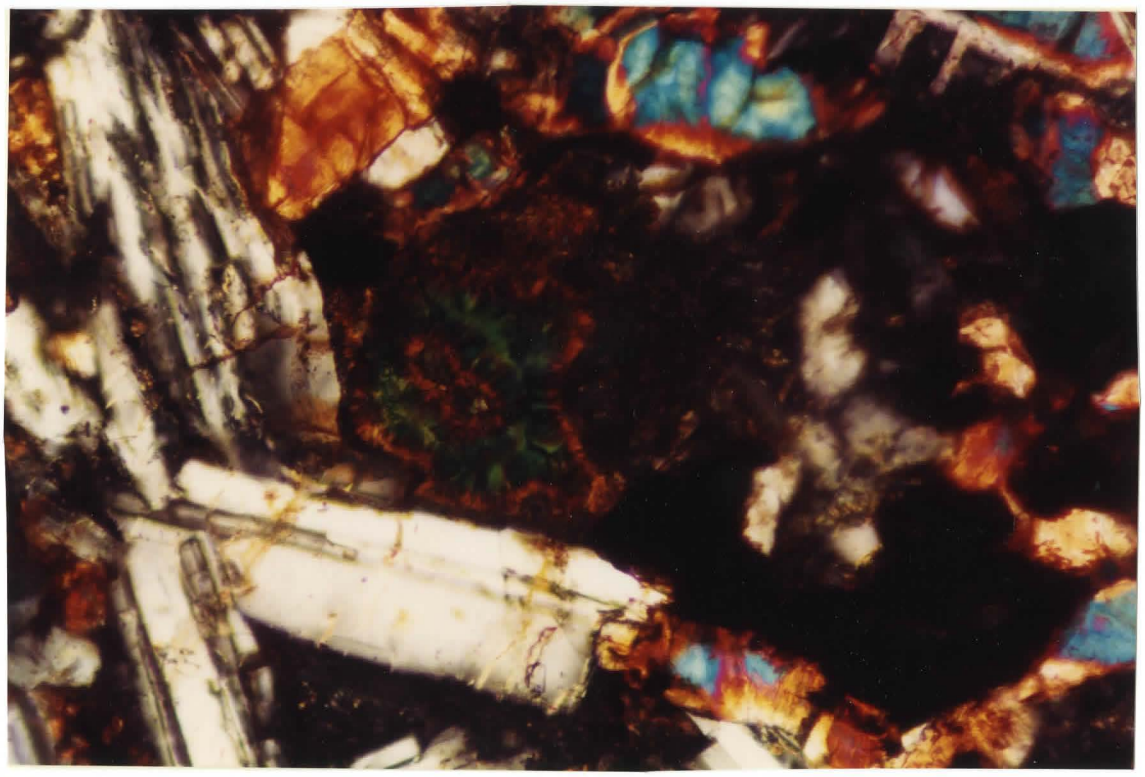

Photomicrograph 5.3e Subophitic texture whereby hypersthene is partially enclosing the plagioclase laths (G-07, magnified 160 times).

Photomicrograph 5.4d Zoned plagioclase crystals. Notice the wide central Ca-rich cores surrounded by narrower Na-rich zones (D-04, magnified 63 times).

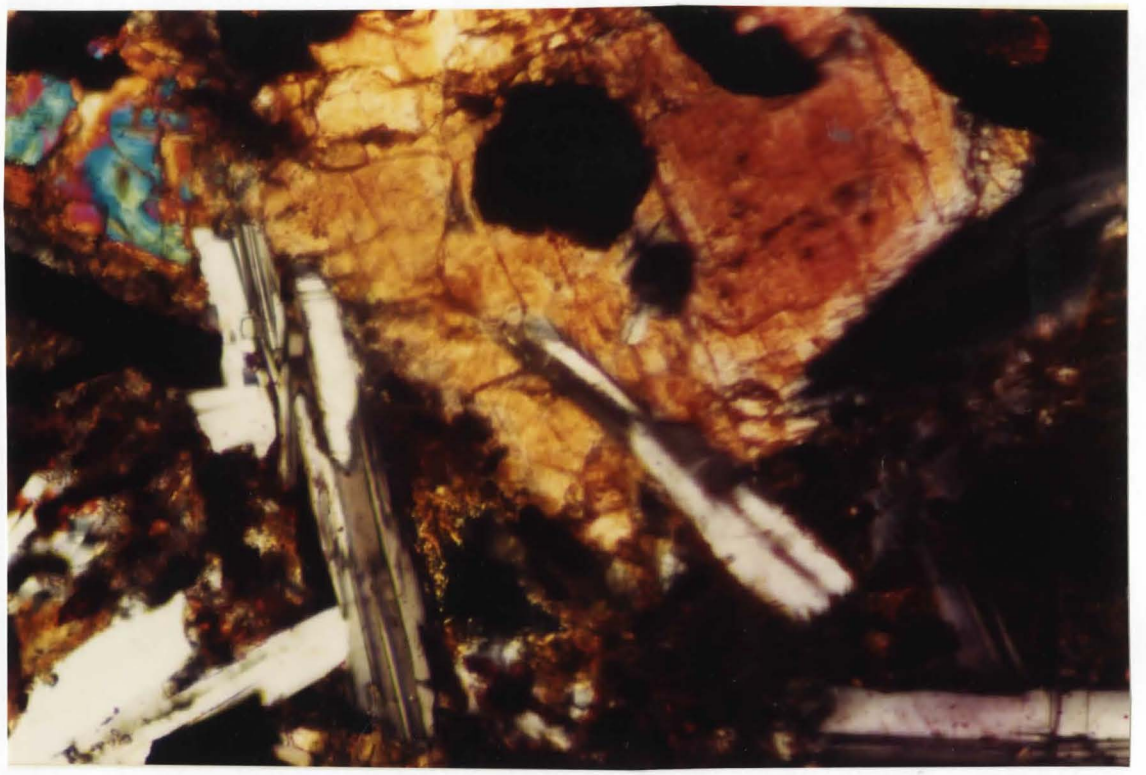

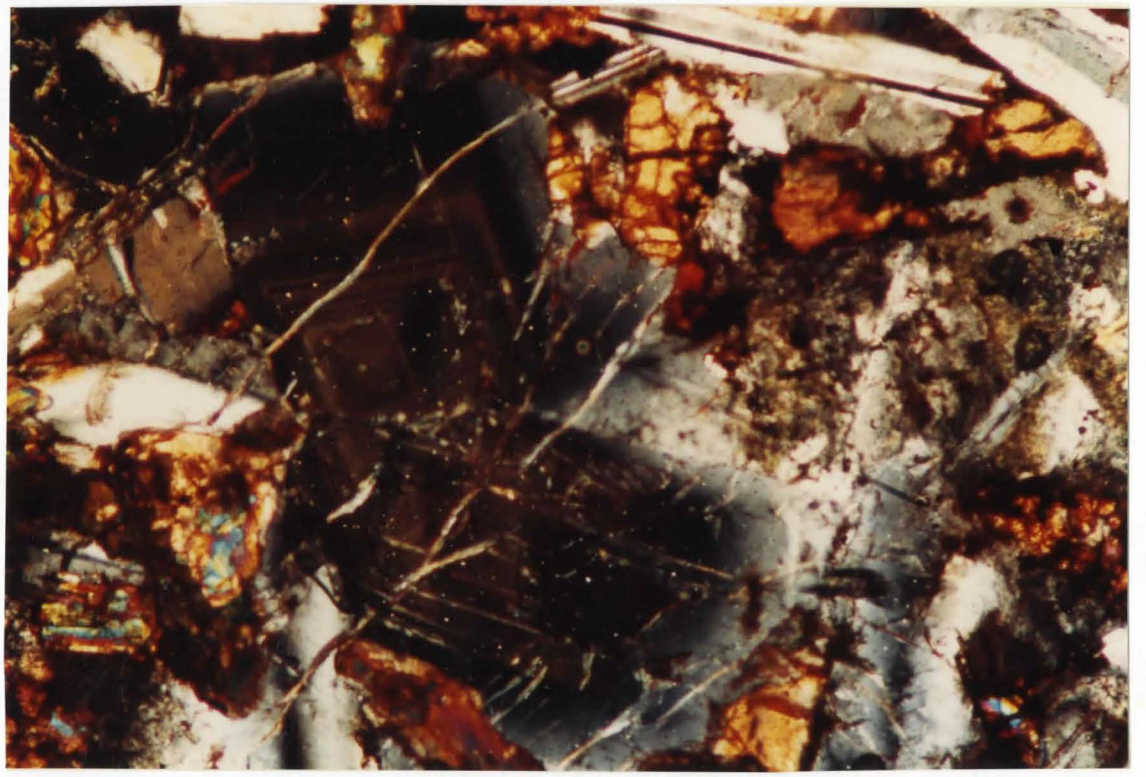

Photomicrograph 5.5e Herring-bone texture displayed by augite (Q-17, magnified 160 times).

Photomicrograph 5.6f Typical crystalline phase-glassy groundmass relationships. Notice altered margins of plagioclase laths (O-15, magnified 160 times).

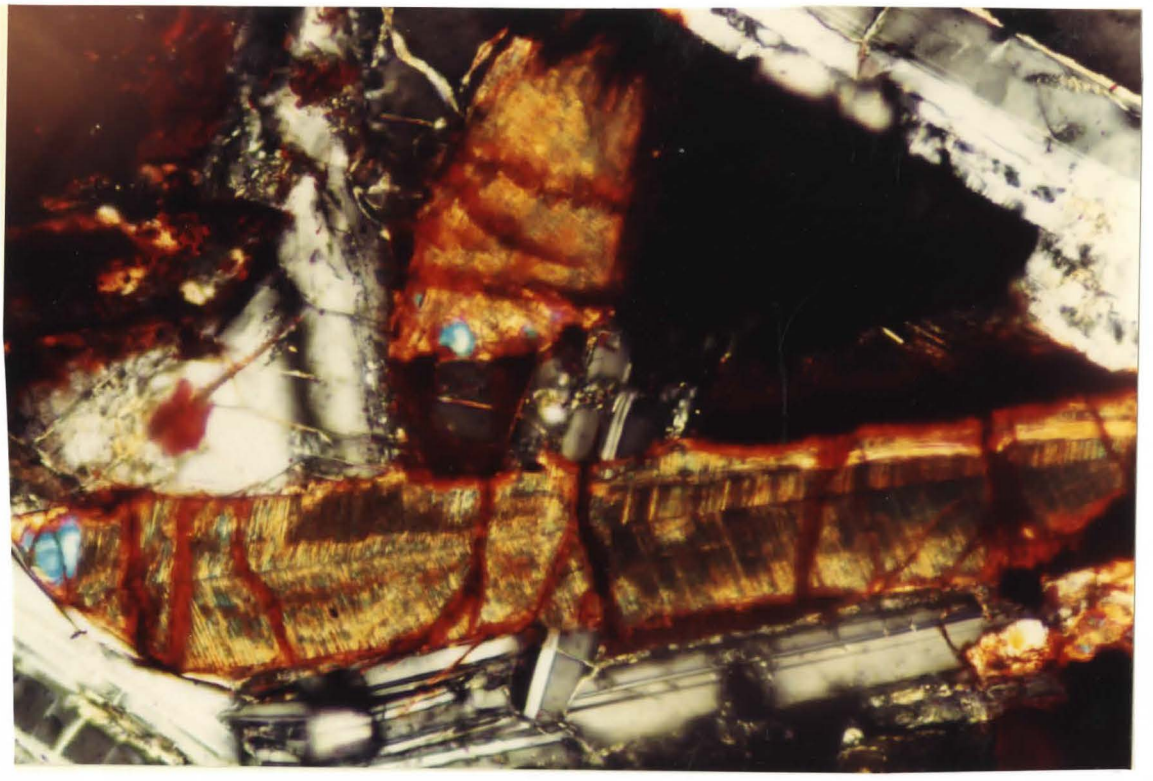

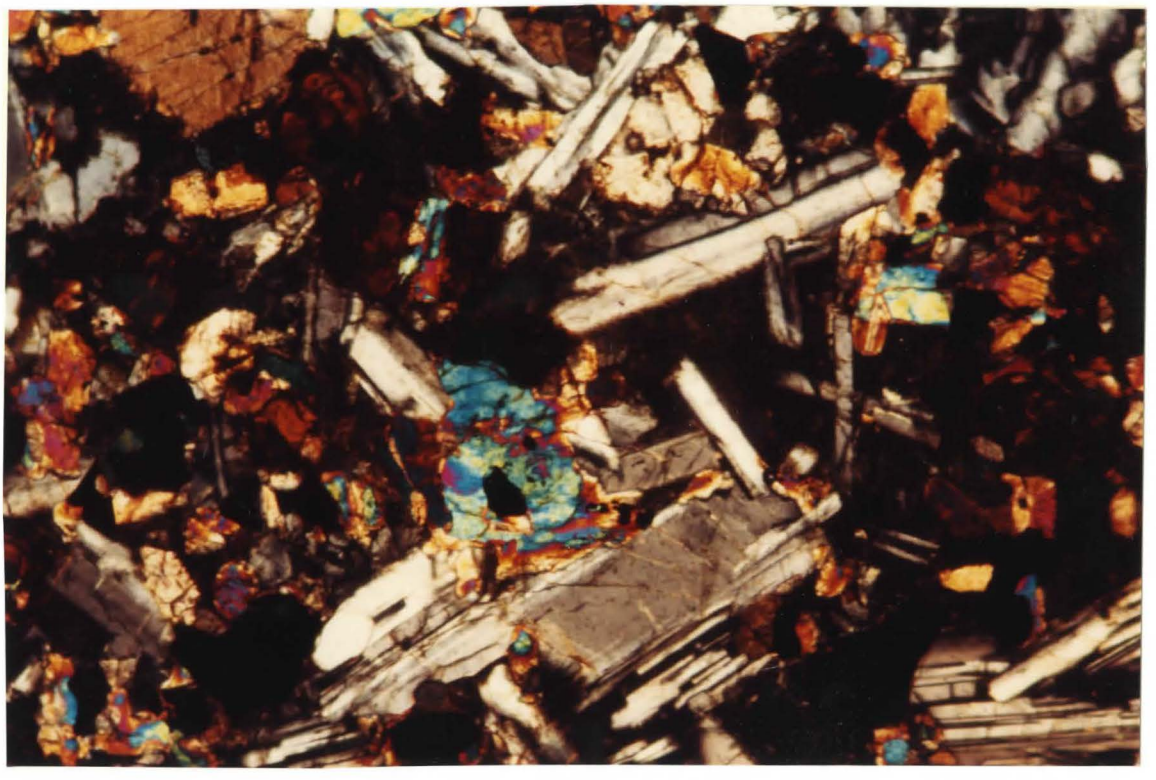

Photomicrograph 5.7g Reddish-brown glassy groundmass (iddingsite) with numerous shards of plagioclase (R-18, magnified 160 times).

Photomicrograph 5.8h Extinction crosses in spherulites (H-08, magnified 160 times).

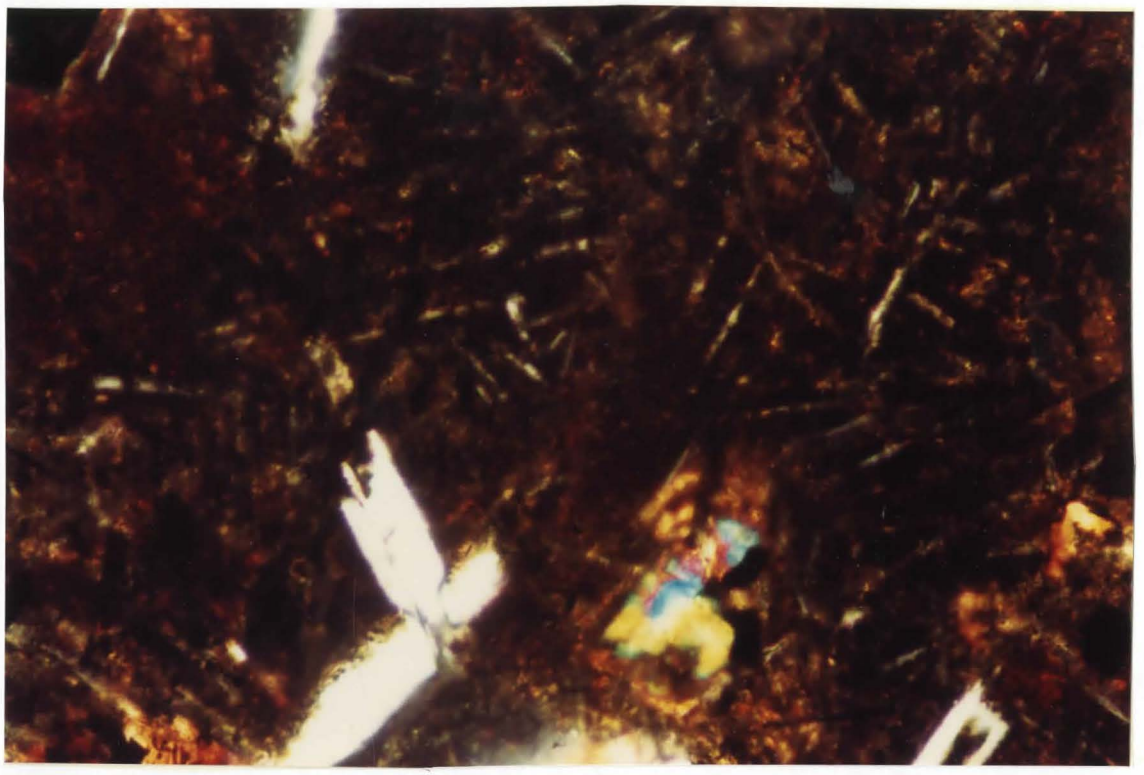

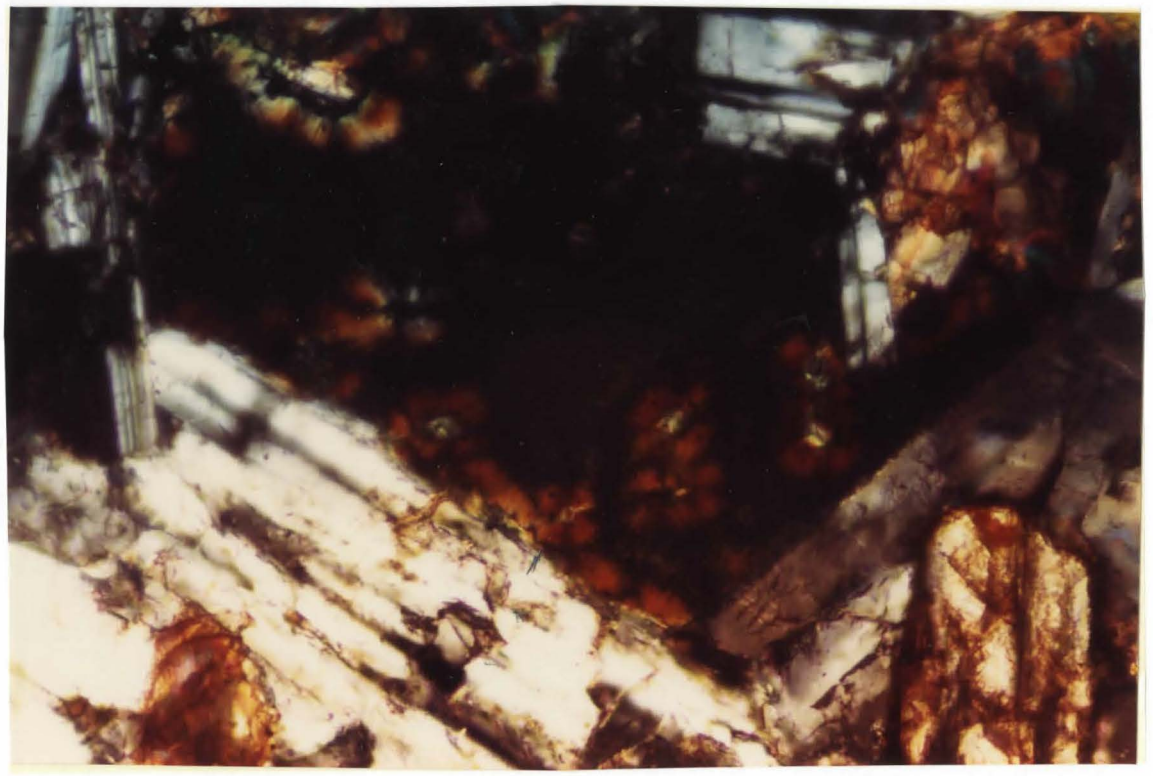

Photomicrograph 5.9i Axiolitic growth pattern displayed by chlorite (L-12, magnified 160 times).

Photomicrograph 5.10j Rare banding of volcanic glass due to flowage (L-12, magnified 63 times).

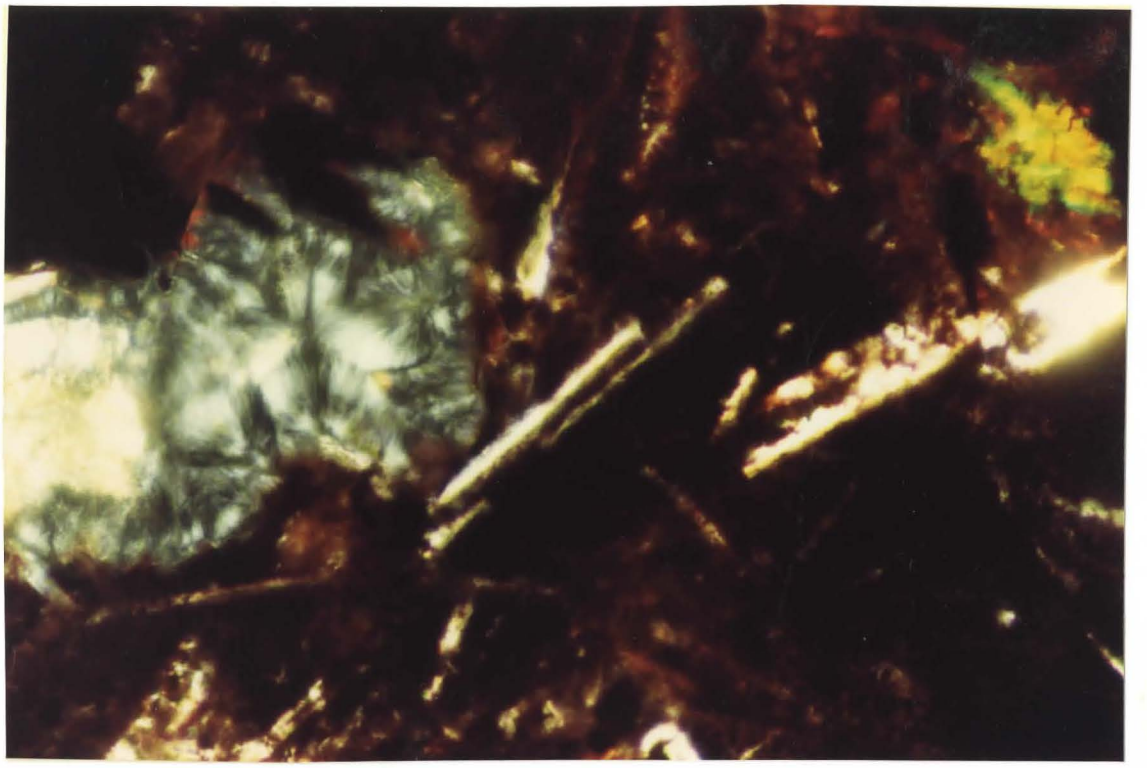

Photomicrograph 5.11k Amorphous chlorite (appears reddish due to use of blue filter) lining a vesicle that has subsequently been infilled by quartz (P-15, magnified 16 times).

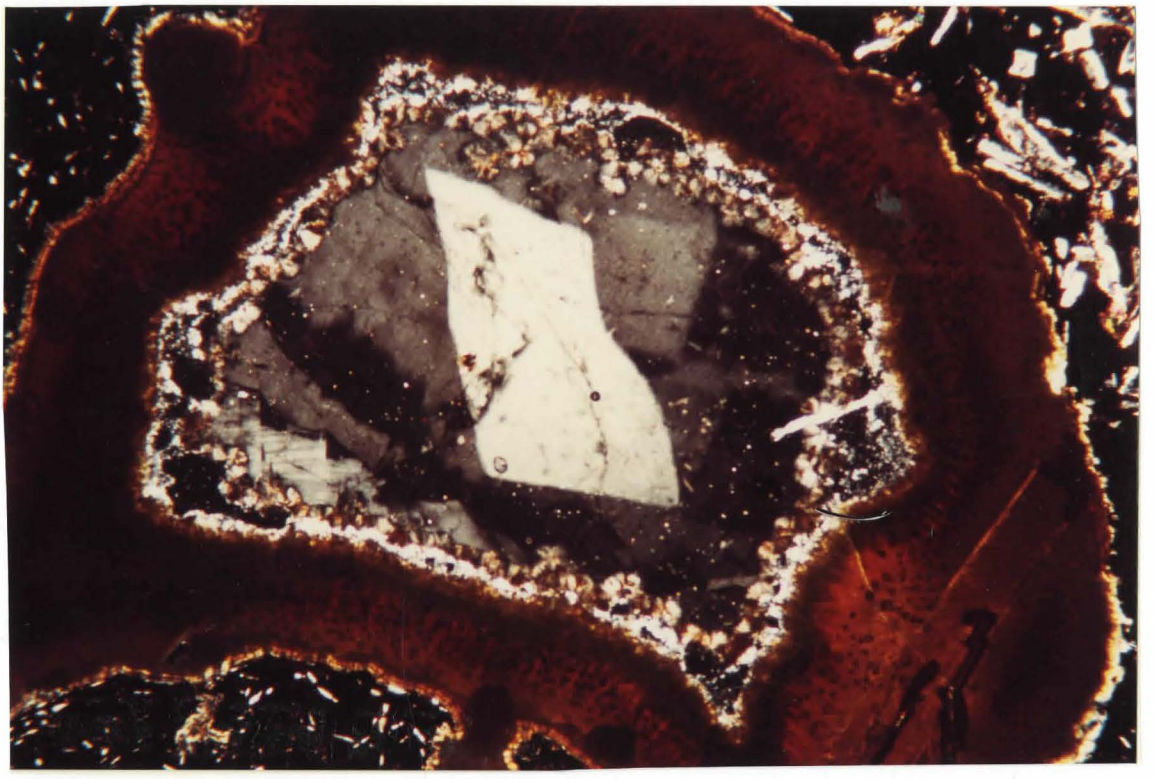

PETROCHEMISTRY OF THE PARANÁ BASALTS

To detect variations in major element chemistry from XRF analyses and C.I.P.W. norms is often difficult. Graphical methods to manipulate these columns of numbers are often employed to detect subtle changes that may otherwise be overlooked. Graphical methods if properly shown on graphs, should trace out curves analogous to paths followed on phase diagrams. Therefore, one possible goal of such graphs is to reveal genetic sequences from the parent liquid through the crystallization history of the rock to the final residual liquid.

Chemical variations of a magma series, such as the Paraná basalts are conventionally displayed on variation diagrams. The Harker diagram (see figure 6.1) is a form of variation diagram whereby the weight percentages of the principal oxides are plotted against SiO_2. One of the prinicipal factors governing the configurations displayed by this type of diagram is fractional crystallization. This is an especially valuable method when dealing with glassy or fine grained rocks which may display liquid lines of descent allowing interpretation of what must be added or subtracted to generate the curves in question.

The Harker diagrams display the following features of the Paraná Basalts:

1) Fe_2O_3 (total Fe) is the most abundant principal oxide in the suite. Therefore, this supports the observation that opaque Fe-oxides were very common in thin section.

FIGURE 6.1

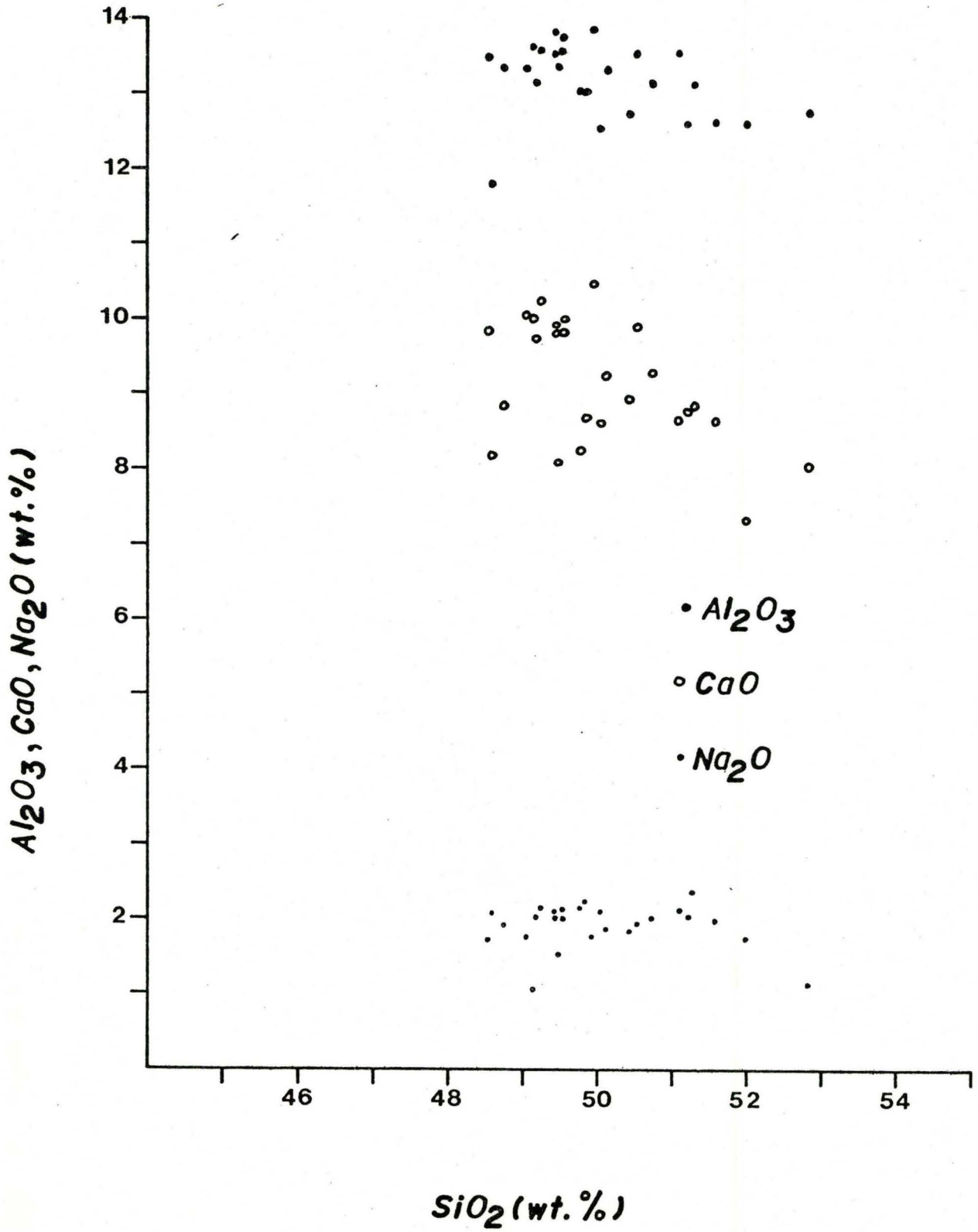
14
12
10
8
6
4
2
46
48
50
52
54
Al_2O_3, CaO, Na_2O (wt.%)
SiO_2 (wt.%)
• Al_2O_3
○ CaO
• Na_2O

FIGURE 6.1

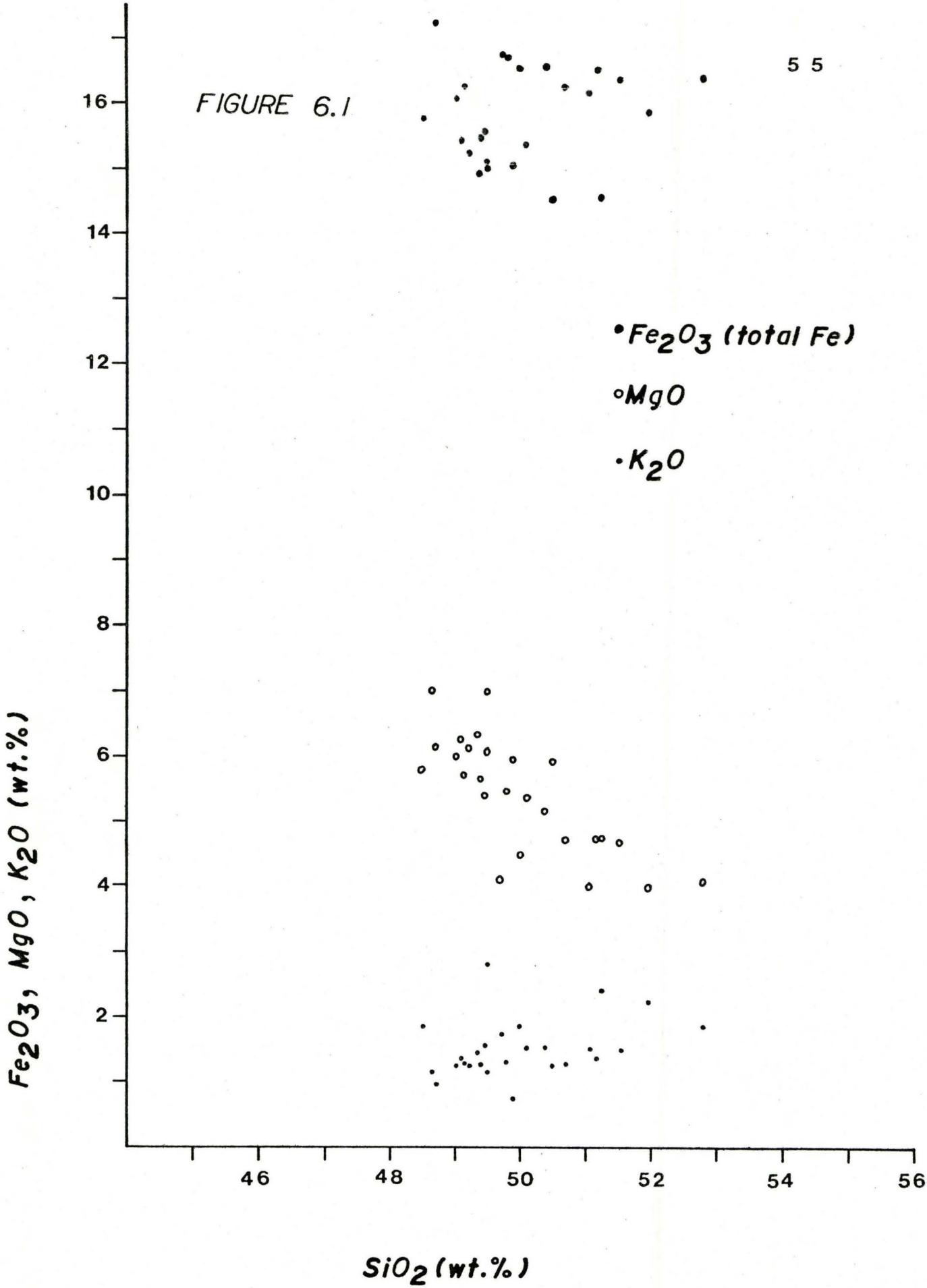
16
14
12
10
8
6
4
2
46
48
50
52
54
56
•Fe2O3 (total Fe)
◦MgO
·K2O
Fe2O3, MgO, K2O (wt.%)
SiO2 (wt.%)

FIGURE 6.2

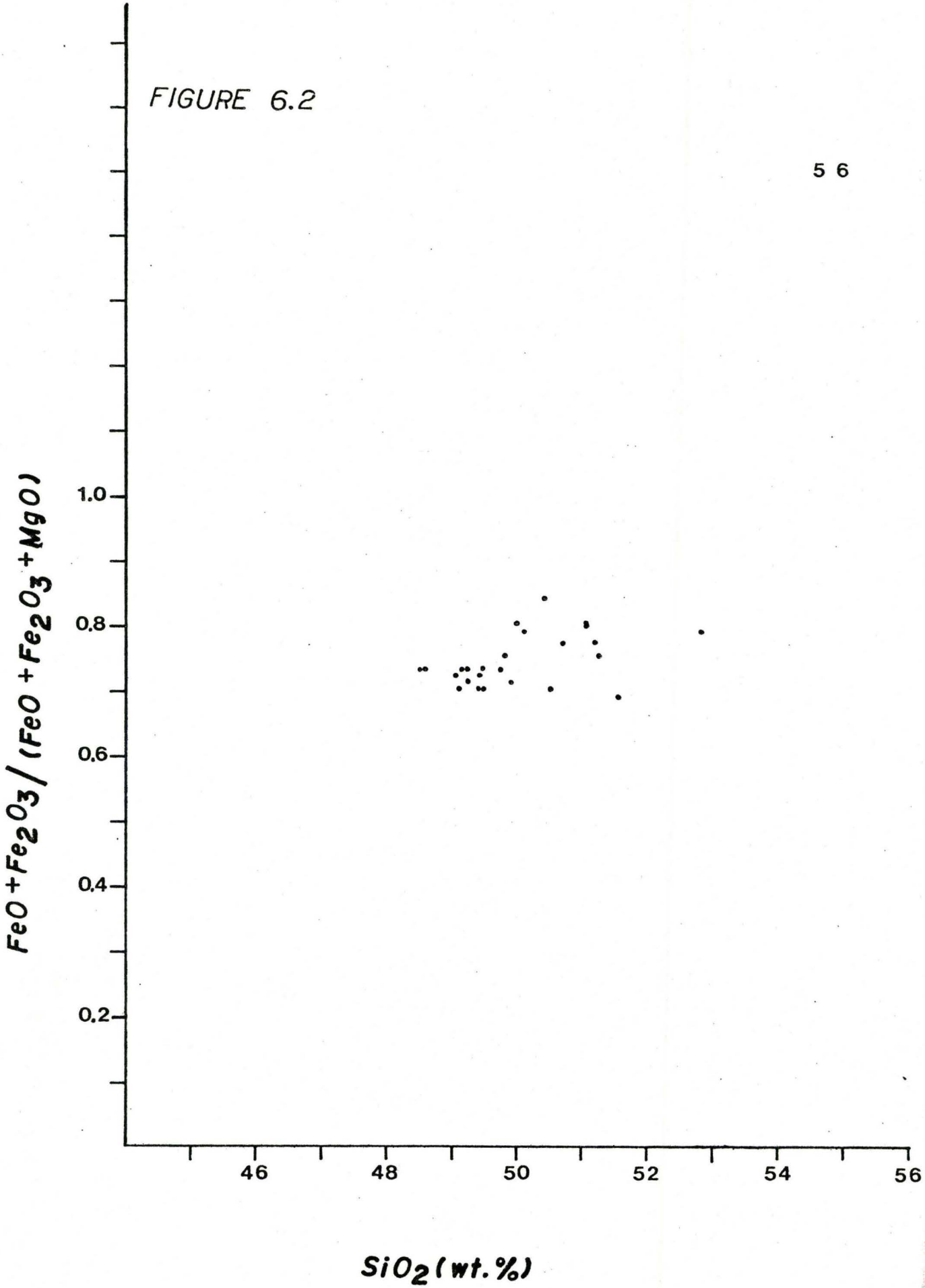

2) Al_2O_3 is the next most abundant oxide and is characteristically confined to a very narrow range. The majority of the samples have Al_2O_3 contents ranging from 12.5 - 13.9 wt.%.

3) CaO is typically found over a broader range. CaO contents range from 8.0 - 10.5 wt.%, and there appears to be a tendancy for CaO contents to decrease with increasing SiO_2 contents.

4) MgO displays characteristics similar to CaO. One difference between these two oxides is that the trend of decreasing MgO contents with increasing SiO_2 contents is better defined.

5) Both Na_2O and K_2O are minor principal oxides ranging from 1.5 - 2.2 wt.% and 1.1 - 1.9 wt.% respectively (for the majority of samples). However, Na_2O is restricted to a narrow range whereas, K_2O displays more variation.

6) From the graph of $FeO + Fe_2O_3/(MgO + Fe_2O_3 + MgO)$, there appears to be very little variation (possibly minor increase with increasing SiO_2 content due to Mg being preferentially incorporated into the ferromagnesian minerals relative to Fe) with increasing SiO_2 contents (see figure 6.2).

As the crystallization of a silicate magma proceeds, the residual liquid becomes enriched in low melting components such as feldspars and ferromagnesian minerals. Thus, Simpson proposed the felsic index $((Na_2O + K_2O) \times 100)/(Na_2O + K_2O + CaO)$ to be plotted against Deer's Mafic index $((FeO + Fe_2O_3) \times 100)/(MgO + FeO + Fe_2O_3)/$ From figures 6.3, it appears that there is a linear relationship between the mafic and felsic indices for this suite of rocks.

From the Ab-An-Or system (see figure 6.4), there appears to be a scattering of points about a central locus. There are two points to be made in regards to this graph:

1) There is a fairly narrow range of Ab-An ratios and,
2) There is more variability in the orthoclase component.

Magmas that are quenched rapidly generally produce very restricted Ab-An ranges. The samples from the Misiones Province all appear to have been rapidly quenched. Their range in Ab-An contents may be the result of fractional crystallization which has operated prior to the final consolidation of the magma.

The AFM diagram illustrated in figure 6.5 displays several prominent features. One observation of the AFM diagram is the spatial confinement of basaltic types to particular zones within the diagram. The Paraná basalts show very little variation within this and are typically an Fe-rich quartz tholeiite and plot in the proximity of the total iron apex. The Paraná basalts are considerably more evolved than the other basaltic types and have characteristically higher FeO/MgO ratios and have higher alkali contents. Mg-rich basalts and peridotites (extremely Mg-rich) plot near the right hand side of the diagram and are characterized by low alkali contents and variable FeO/MgO ratios. The effect of alkali element mobility which could alter results must be assessed when plotting peridotites and Archean rocks in AFM diagrams. Al-rich basalts are generally enriched in alkalis relative to the Mg-rich basalts and display FeO/MgO ratios approximating unity and plot in the central region of the

FIGURE 6.3

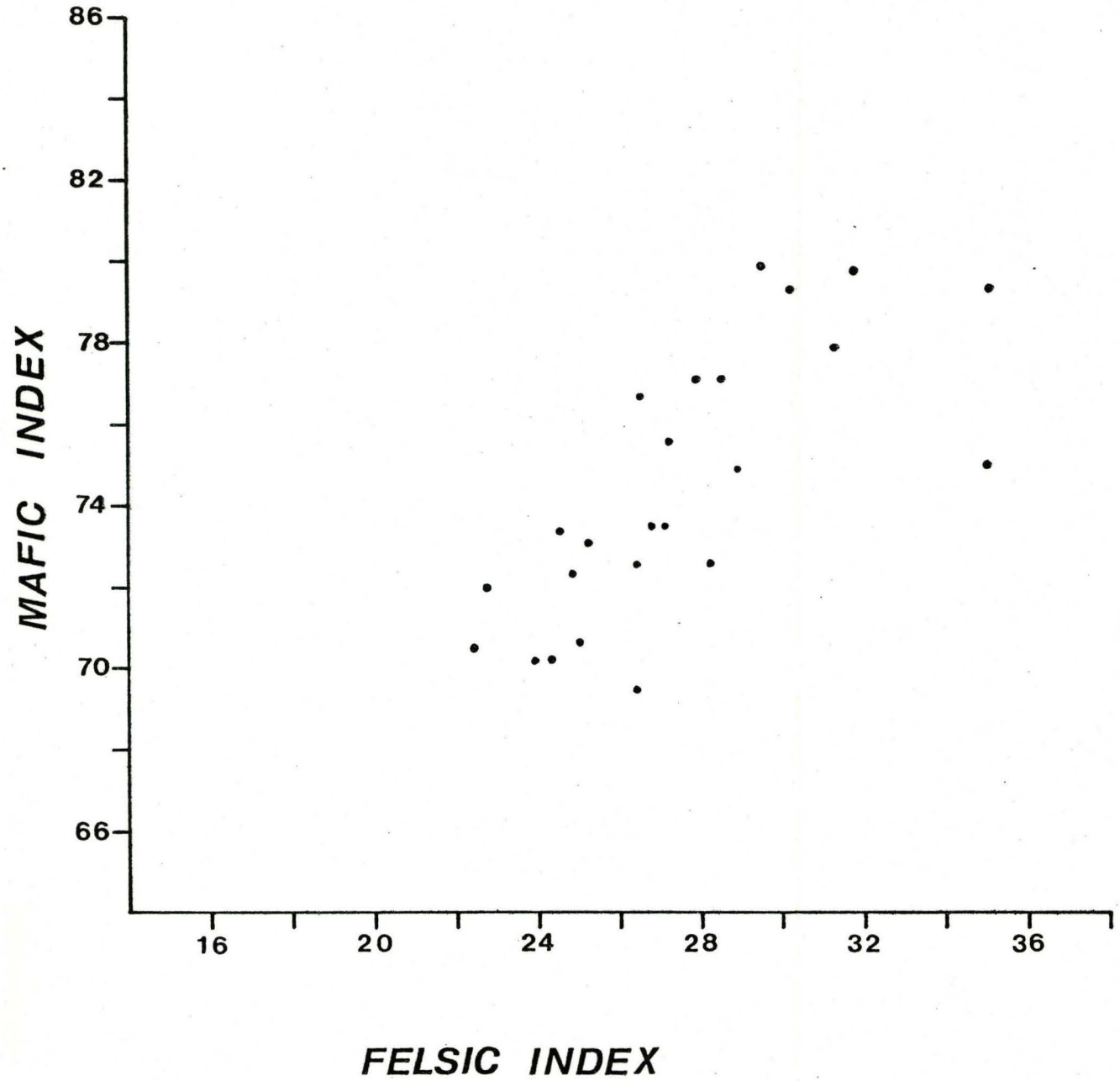

FIGURE 6.4 Triangular plot of Ab-An-Or.

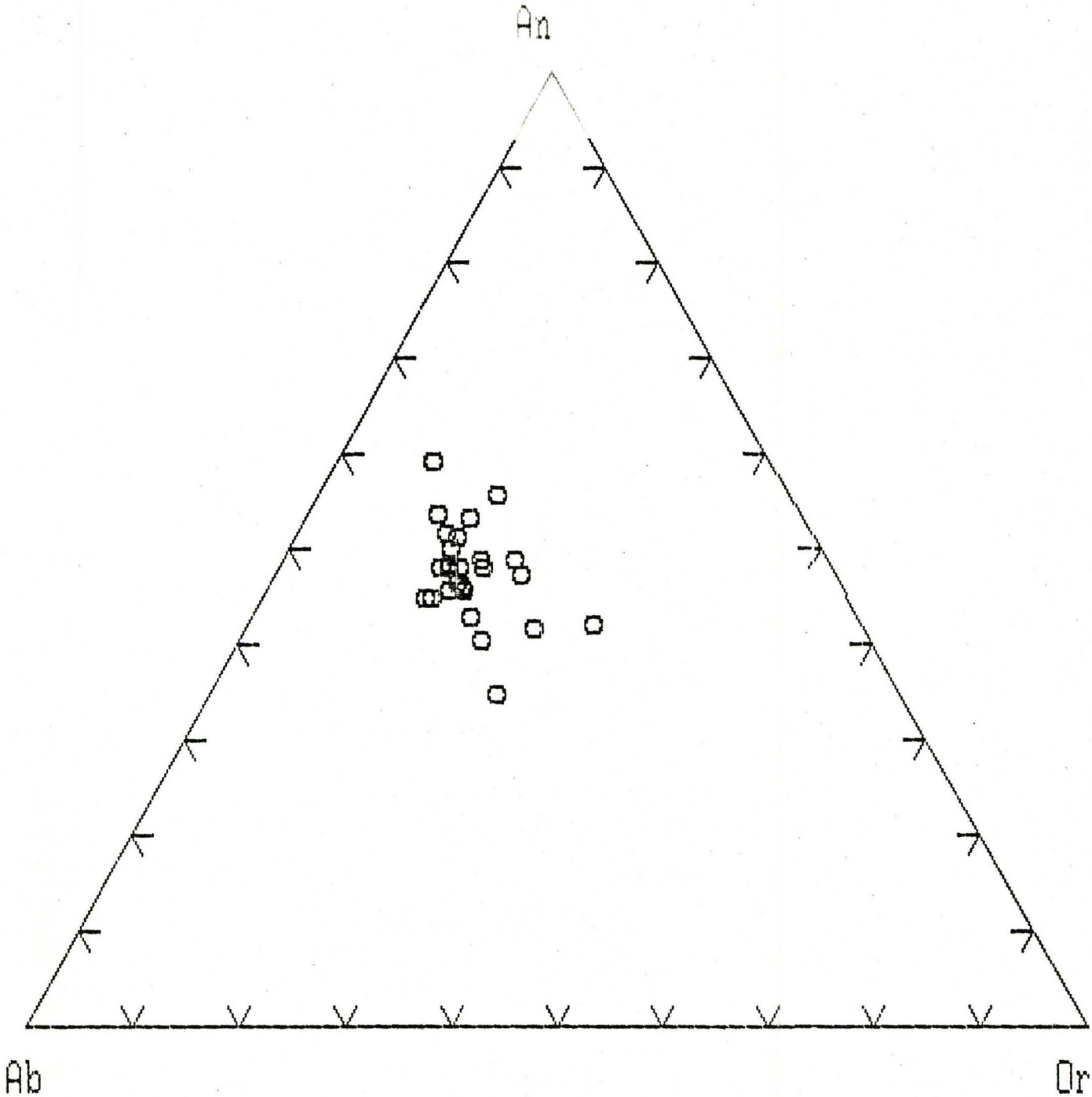

FIGURE 6.5 AFM diagram.

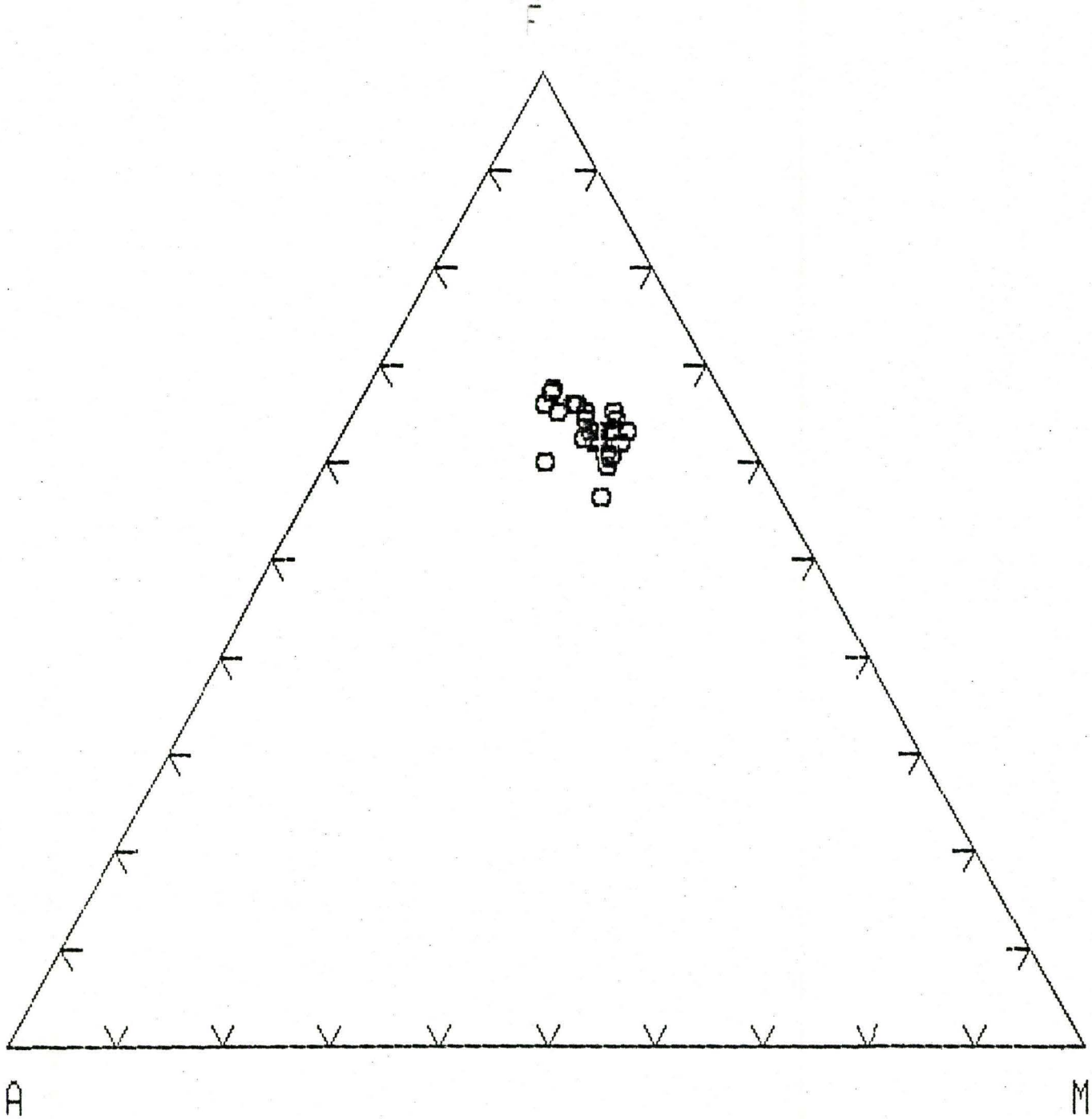

diagram. Alkali rich basalts are similar to Al-rich basalts with respect to their FeO/MgO ratios but are enriched in K_2O and plot on the left hand side of the diagram.

The division of the AFM diagram into zones of basaltic compositions are due to variations in the ratios of MgO/(MgO + FeO), $K_2O/(K_2O + Na_2O)$ and NaO/(Na_2O + Ca_2O). These variations may be accounted for by considering the sequence of minerals formed during progressive crystallization of the magma. Mg tends to be preferentially incorporated in ferromagnesium phases relative to ferrous iron and the residual liquid becomes progressively iron enriched relative to magnesium. Plagioclase is similar in this respect and preferentially incorporates Ca producing a residual liquid enriched in Na and K.

There are no broad spatial trends that are exhibited from sample to sample, but there are geographic regions which display anomalous values when compared to the mean. The following variations were observed:

Posadas - San Ignacio Region

a) This region displayed enrichment of FeO and MgO and,

b) This region is depleted in Al_2O_3, Fe_2O_3, and K_2O.

Garuhape - Eldorado Region

a) This region is depleted in SiO_2.

San Martin Cataratas Region

a) This region is enriched in P_2O_5 and depleted in MnO.

General Güemes - San Javier Region

a) This region is enriched in Al_2O_3, MgO and CaO and,

b) This region is depleted in FeO, Fe_2O_3, and K_2O.

Garruchos Region

a) This region is enriched in Na_2O and K_2O and,

b) This region is depleted in K_2O, TiO_2 and P_2O_5.

CONCLUSIONS

The quartz tholeiites of the Misiones Province are characteristically uniform in several respects despite the vast geographic sampling area. The key points that should be emphasized are:

1) In order to account for the spatial uniformity of these quartz tholeiites, it can be assumed that individual eruptions have been characterized by large volumes which are quite areally extensive.

2) Mineralogically, these quartz tholeiite are remarkably similar and the only petrographic variation appears to be the crystalline phase:glass ratio.

3) The FeO/Fe_2O_3 ratio appears to be an important variable in determining the relative abundances and varieties of groundmass constituents.

4) Late stage and/or deuteric alteration appears to have been a viable operating mechanism in the majority of the samples.

5) Fractional crystallization appears to have been a viable mechanism which has operated throughout the crystallization history of these samples. However, there is very little evidence based on petrography and petrochemistry that fractional crystallization and/or crystal accumulation has operated throughout this suite to produce major variations from sample to sample.

6) The petrochemistry of this suite displays only minor spatial variations and there is not an overall progression from more primitive to more evolved lavas with time.

7) The dike system in the Misiones Province may have provided pathways for the magmas ascent to the surface but it seems unlikely that there has been high-level crustal storage of magma. This is based upon the fact that the effects of fractional crystallization throughout this suite are minimal.

APPENDIX 1A

TITRIMETRIC DETERMINATION OF FERROUS IRON

The modified Pratt Method of hot acid decomposition was applied to determine the percentage of ferrous iron in the sample. This procedure was required as XRF analyses did not differentiate between the ferrous and ferric states and simply analyzed for total iron.

Procedure:

1. Weigh 0.500 g of sample (approximately 100 mesh) and transfer it into a platinum crucible equipped with a tight fitting cover.

2. Add 10ml of H_2SO_4 (18M) to the platinum crucible and swirl gently to prevent the sample from caking to the bottom of the crucible.

3. Add 5ml of HF to the platinum crucible and place the platinum crucible on a silica triangle over a bunsen burner with a low flame and then cover the crucible.

4. Allow the contents of the crucible to boil gently for 10 minutes. Do not allow the contents to boil vigorously or for extended periods of time because water will start to evaporate and H_2SO_4 will begin to oxidize the ferrous iron.

5. Add 450ml of distilled water, 50ml of 5% (saturated) boric acid solution and 15ml H_2SO_4 (18M) to a 600ml Pyrex beaker.

6. At the conclusion of the heating period, place the platinum crucible directly into the 600ml Pyrex beaker using platinum tipped crucible tongs. Rinse the condensation droplets on the crucible's cover with distilled water into the 600ml Pyrex beaker.

7. Place a magnetic stirring rod in the platinum crucible to ensure that the sample solution is homogeneous.

8. Titrate the solution with $K_2Cr_2O_7$ (10M).

Determining the percentage of FeO in the sample was calculated using the following expression;

$$\%FeO = \frac{\text{ml of titrant x molality}}{1000} \times \frac{71.85}{1} \times \frac{100}{\text{sample wt.(g)}}$$

The percentage of Fe_2O_3 was determined in the C.I.P.W. program using the following expression;

$$\%Fe_2O_3 = Fe_2O_{3_T} - 1.096(FeO) \text{ where}$$

$Fe_2O_{3_T}$ = total iron determined by XRF analysis.

APPENDIX 2B

THE C.I.P.W. NORM

Chemical analyses are expressed as weight percentages of oxides but due to the large number of oxides involved (11 in this case), comparison of samples may be difficult. The C.I.P.W.* norm analysis manipulates the oxide components into a smaller number of variables analogous to potential minerals which could form if the rock crystallized completely under ideal conditions. These potential minerals in common basaltic rocks are the feldspars, pyroxenes, olivines, ilmenite, magnetite, apatite and sometimes nepheline or quartz. Solid solution series that exist in the feldspars, pyroxenes and olvines are calculated in terms of their end-members which may be recalculated as normative compositions (the normative feldspar composition may be expressed as percentages of An, Ab and Or).

The first step of the C.I.P.W. calculation involves the weight percent of each oxide to be recast into molecular proportions (weight percent/molecular weight). The molecular proportions of each oxide are then systematically consumed in a standard order, first by assigning all the P_2O_5 to apatite and a corresponding amount of CaO to yield the appropriate apatite formula. Equal amounts of TiO_2 and FeO are then consumed to form ilmenite. This process is continued until hypersthene is formed, at which point a summation of the silica

* named for its inventors, Cross, Iddings, Pirsson and Washington (1903).

consumed is performed. If the starting molecular proportion of silica is greater than the amount consumed, the rock is oversaturated with respect to silica and quartz appears in the norm. However, if the starting molecular proporiton of silica is less than the amount consumed, some of the MgO and FeO assigned to hypersthene must be recaluculated to form the less siliceous mineral olivine. This process continues for nepheline and leucite in silica undersaturated rocks until an appropriate silica balance has been achieved.

These are the general guidelines followed in calculating C.I.P.W. normative minerals (a list of normative minerals calculated in the C.I.P.W. computer program appears in table 3C-1). However, this, is a very time consuming process that may be implemented by the use of accepted C.I.P.W. computer programs. The C.I.P.W. computer program applied in calculating the normative compositions was written by G. David Mattison of the department of geochemistry and mineralogy of the Pennsylvania State University.

TABLE 3C-1
C.I.P.W. NORMATIVE CONSTITUENTS AND THEIR OXIDE COMPONENTS

Oxide Components		Normative Constituents			
Formula	Mol.Wt.*	Name	abbrev.	Mol.Wt.*	Formula
SiO_2	60.09	Quartz	q	60.09	SiO_2
TiO_2	79.90	Corundum	c	101.96	Al_2O_3
Al_2O_3	101.96	Orthoclase	or	556.70	$K_2O-Al_2O_3-6SiO_2$
Fe_2O_3	159.69	Albite	ab	524.48	$Na_2O-Al_2O_3-6SiO_2$
FeO	71.85	Anorthite	an	278.22	$CaO-Al_2O_3-2SiO_2$
MnO	70.94	Leucite	lc	436.52	$K_2O-Al_2O_3-4SiO_2$
MgO	40.30	Nepheline	ne	284.12	$Na_2O-Al_2O_3-2SiO_2$
CaO	56.08	Kaliophilite	kp	316.34	$K_2O-Al_2O_3-2SiO_2$
Na_2O	61.98	Acmite	ac	462.03	$Na_2O-Fe_2O_3-4SiO_2$
K_2O	94.20	Sodium Metasilicate	ns	122.07	Na_2O-SiO_2
P_2O_5	141.95	Potassium Metasilicate	ks	154.29	K_2O-SiO_2
		Wollastonite	wo	116.17	$CaO-SiO_2$
		Diopside	di		
		Diopside	di-di	216.56	$CaO-MgO-2SiO_2$
		Hedenbergite	di-hd	248.11	$CaO-FeO-2SiO_2$
		Hypersthene	hy		
		Enstatite	hy-en	100.39	$MgO-SiO_2$
		Ferrosilite	hy-fs	131.94	$FeO-SiO_2$
		Olivine	ol		
		Forsterite	ol-fo	140.69	$2MgO-SiO_2$
		Fayalite	ol-fa	203.79	$2FeO-SiO_2$
		Calcium Orthosilicate	cs	172.25	$2CaO-SiO_2$
		Magnetite	mt	231.54	$FeO-Fe_2O_3$
		Ilmenite	il	151.75	$FeO-TiO_2$
		Hematite	hm	159.69	Fe_2O_3
		Sodium Carbonate	nc	105.99	Na_2O-CO_2
		Rutile	ru	79.90	TiO_2
		Apatite	ap	336.22	$3CaO-P_2O_5-1/3CaF_2$
		Calcite	cc	100.09	$CaO-CO_2$

*Molecular weights are based on the 1975 scale of atomic weights, in which $^{12}C=12.000$, as tabulated in Robie and others (1978).

APPENDIX 3C

MODAL COMPOSITIONS

Sample A-01

(40%) Plagioclase - An_{47} (Michel Lèvy), 0.423 (C.I.P.W. albite ratio).
(20%) Augite - anhedral to subhedral, commonly colour zoned.
(5%) Hypersthene - anhedral to subhedral, relatively large (0.4x0.4mm).
(18%) Volcanic Glass - devitrified, reddish-brown, perlite, spherulites.
(10%) Chlorite - interstitial, associated with volcanic glass, spherulites.
(1-2%) Quartz - subhedral, often displayed stained borders.
(4-5%) Fe-Oxides - anhedral to subhedral, variable size, interstitial.
$FeO/Fe_2O_3 = 0.99$

Sample B-02

(40%) Plagioclase - An_{50} (Michel Lèvy), 0.448 (C.I.P.W. albite ratio).
(15%) Augite - subhedral, commonly colour zoned.
(2-3%) Hypersthene - anhedral to subhedral, variable size.
(26%) Volcanic Glass - devitrified, reddish-brown, numerous microphenocrysts.
(7-8%) Chlorite - interstitial, often associated with volcanic glass.
(2-3%) Quartz - anhedral, fractured. Wavy to undulatory extinction.
(5%) Fe-oxides - anhedral, variable size, minor hematite staining.
$FeO/Fe_2O_3 = 0.63$

Sample C-03

(35%) Plagioclase - An_{57} (Michel Lèvy), 0.462 (C.I.P.W. albite ratio).
(15%) Augite - large (0.3x0.3mm), subhedral, colour zoned phenocrysts.
(2-3%) Hypersthene - small, subhedral, interstitial.
(29%) Volcanic Glass - devitrified, altering associated minerals.
(10%) Chlorite - interstitial, associated with volcanic glass.
(2-3%) Quartz - anhedral to subhedral, often found interstitially.
(5%) Fe-oxides - small, anhedral, minor hematite staining.
$FeO/Fe_2O_3 = 0.55$

Sample D-04

(35%) Plagioclase - An_{46} (Michel Lèvy), 0.408 (C.I.P.W. albite ratio).
(15%) Augite - anhedral, colour zoned, minor hematite staining.
(3-4%) Hypersthene - subhedral, some crystals display schiller textures.
(28%) Volcanic Glass - devitrified, numerous microphenocrysts.
(10%) Chlorite - interstitial, associated with volcanic glass.
(2-3%) Quartz - anhedral, recrystallized mosaics lining vesicles.
(5%) Fe-oxides - large, anhedral, variable size, interstitial.
$FeO/Fe_2O_3 = 0.67$

Sample E-05

(40%) Plagioclase - An_{57} (Michel Lèvy), 0.434 (C.I.P.W. albite ratio).
(20%) Augite - anhedral, colour zoned, minor green (chlorite) staining.
(3-4%) Hypersthene - small, anhedral, altering to groundmass.
(19%) Volcanic Glass - devitrified, altering associated minerals.
(7-8%) Chlorite - interstitial, commonly associated with volcanic glass.
(2-3%) Quartz - anhedral to subhedral. Wavy and undulatory extinction.
(7-8%) Fe-oxides - anhedral, interstitial, variable sizes.
$FeO/Fe_2O_3 = 0.50$

Sample F-06

(40%) Plagioclase - An_{54} (Michel Lèvy), 0.401 (C.I.P.W. albite ratio).
(15%) Augite - anhedral to subhedral, colour zoned.
(3-4%) Hypersthene - anhedral to subhedral. Rare euhedral faces.
(23%) Volcanic Glass - devitrified, reddish-brown, numerous microphenocrysts.
(7-8%) Chlorite - interstitial, associated with volcanic glass.
(2-3%) Quartz - small, anhedral. Wavy and undulatory extinction.
(7%) Fe-oxides - anhedral, interstitial, hematite staining is common.
$FeO/Fe_2O_3 = 0.52$

Sample G-07

(35%) Plagioclase - An_{57} (Michel Lèvy), 0.427 (C.I.P.W. albite ratio).
(10%) Augite - small (0.1x0.1mm) subhedral crystals. Rare euhedral crystals.
(2-3%) Hypersthene - small, variable size, subhedral, rare euhedral faces.
(36%) Volcanic Glass - devitrified, numerous microphenocrysts.
(7-8%) Chlorite - lining vesicles in a radiating pattern.
(2-3%) Quartz - small, anhedral, microcrystalline mosaics lining vesicles.
(5%) Fe-oxides - small, interstitial, anhedral to subhedral.
$FeO/Fe_2O_3 = 0.49$

Sample H-08

(40%) Plagioclase - An_{57} (Michel Lèvy), 0.371 (C.I.P.W. albite ratio).
(20%) Augite - small subhedral crystals. Size is quite variable.
(3-4%) Hypersthene - small, variable size, subhedral.
(21%) Volcanic Glass - devitrified, reddish-brown, altering associated minerals.
(7-8%) Chlorite - interstitial, lining vesicles.
(2-3%) Quartz - small, anhedral, interstitial.
(7-8%) Fe-oxides - anhedral, interstitial, minor hematite staining.
$FeO/Fe_2O_3 = 0.71$

Sample I-09

(40%) Plagioclase - An_{47} (Michel Lèvy), 0.332 (C.I.P.W. albite ratio).
(15%) Augite - large (1.5x1.5mm) anhedral crystals, colour zoned.
(2-3%) Hypersthene - small, anhedral. Size is quite variable.
(24%) Volcanic Glass - devitrified, reddish-brown, altering associated minerals.
(7-8%) Chlorite - interstitial, spherulites and axiolites.
(1-2%) Quartz - anhedral crystals, interstitial.
(7-8%) Fe-oxides - anhedral, interstitial, hematite staining is common.
$FeO/Fe_2O_3 = 0.60$

Sample J-10

(40%) Plagioclase - An_{55} (Michel Lèvy), 0.400 (C.I.P.W. albite ratio).
(20%) Augite - subhedral, variable sizes.
(5%) Hypersthene - anhedral to subhedral, altering to groundness.
(17%) Volcanic Glass - devitrified, spherulites, altering associated minerals.
(10%) Chlorite - interstitial, spherulites, commonly associated in volcanic glass.
(2-3%) Quartz - small, anhedral. Often found as microphenocrysts in volcanic glass.
(5%) Fe-oxides - large but variable sizes, very minor hematite staining.
$FeO/Fe_2O_3 = 1.14$

Sample K-11

(45%) Plagioclase - An_{50} (Michel Lèvy), 0.475 (C.I.P.W. albite ratio).
(15%) Augite - small (0.2x0.2mm), anhedral, subhedral.
(2-3%) Hypersthene - variable size, subhedral, altering to groundmass.
(16%) Volcanic Glass - devitrified, axiolites, numerous microphenocrysts.
(10%) Chlorite - interstitial, axiolites, often associated with volcanic glass.
(2-3%) Quartz - small, anhedral, undulatory extinction.
(7-8%) Fe-oxides - small, anhedral, often found as microphenocrysts in volcanic glass.
$FeO/Fe_2O_3 = 0.77$

Sample L-12

(40%) Plagioclase - An_{52} (Michel Lèvy), 0.428 (C.I.P.W. albite ratio).
(15%) Augite - variable size, anhedral to subhedral.
(3-4%) Hypersthene - subhedral, hypersthene laths also present.
(20%) Volcanic Glass - devitrified, spherulites, minor flow banding.
(12-13%) Chlorite - interstitial, commonly associated with volcanic glass.
(2-3%) Quartz - anhedral, some recrystallized mosiacs of quartz.
(5%) Fe-oxides - variable size, anhedral, interstitial.
$FeO/Fe_2O_3 = 1.02$

Sample M-13

(40%) Plagioclase - An_{54} (Michel Lèvy), 0.391 (C.I.P.W. albite ratio).
(10%) Augite - anhedral to subhedral, some large phenocrysts.
(5%) Hypersthene - anhedral, altering to groundmass.
(29%) Volcanic Glass - devitrified, reddish-brown colour.
(4-5%) Chlorite - associated with groundmass.
(2-3%) Quartz - microcrystalline, often lining vesicles.
(7-8%) Fe-Oxides - anhedral, interstitial, minor hematite staining.
$FeO/Fe_2O_3 = 0.28$

Sample N-14

(35%) Plagioclase - An_{55} (Michel Lèvy), 0.441 (C.I.P.W. albite ratio).
(15%) Augite - anhedral phenocrysts, sometimes elongate.
(2-3%) Hypersthene - anhedral, altering to groundmass.
(24%) Volcanic Glass - devitrified, spherulites present.
(15%) Chlorite - interstitial, often lining vesicles.
(2-3%) Quartz - associated with vesicles, wavy extinction.
(5%) Fe-Oxides - variable size, anhedral, interstitial.
$FeO/Fe_2O_3 = 0.76$

Sample O-15

(35%) Plagioclase - An_{52} (Michel Lèvy), 0.337 (C.I.P.W. albite ratio).
(15%) Augite - anhedral, minor alteration, sometimes associated with glassy groundmass.
(5%) Hypersthene - large subhedral phenocrysts, euhedral crystals rare.
(32%) Volcanic Glass - devitrified, reddish-brown, numerous microphenocrysts.
(5%) Chlorite - fibrous, lining vesicles, rarely associated with volcanic glass.
(2-3%) Quartz - small, single anhedral crystals.
(5%) Fe-Oxides - anhedral, interstitial, minor hematite staining.
$FeO/Fe_2O_3 = 0.32$

Sample P-16

(40%) Plagioclase - An_{59} (Michel Lèvy), 0.396 (C.I.P.W. albite ratio).
(20%) Augite - subhedral, some larger phenocrysts.
(3-4%) Hypersthene - small, anhedral. Some larger subhedral phenocrysts.
(20%) Volcanic Glass - devitrified, altering surrounding minerals.
(7-8%) Chlorite - interstitial (rare), lining vesicles, spherulites.
(2-3%) Quartz - anhedral, small. Often associated with vesicles.
(5%) Fe-oxides - interstitial, anhedral, hematite staining is common.

$FeO/Fe_2O_3 = 0.69$

Sample Q-17

(40%) Plagioclase - An_{55} (Michel Lèvy), 0.472 (C.I.P.W. albite ratio).
(15%) Augite - subhedral, some larger pheocrysts, herring-bone texture.
(5%) Hypersthene - small, anhedral, some alteration when associated with volcanic glass.
(26%) Volcanic Glass - devitrified, spherulites, reddish-brown colour.
(5%) Chlorite - fibrous, portions often hematite stained.
(3-4%) Quartz - subhedral, fractured, interstitial, some euhedral faces.
(5%) Fe-oxides - anhedral, interstitial, hematite staining is common.

$FeO/Fe_2O_3 = 0.33$

Sample R-18

(35%) Plagioclase - An_{52} (Michel Lèvy), 0.388 (C.I.P.W. albite ratio).
(15%) Augite - small, anhedral. Some larger, subhedral phenocrysts.
(5%) Hypersthene - anhedral, often altered when associated with volcanic glass.
(23%) Volcanic Glass - devitrified, numerous microphenocrysts.
(12-13%) Chlorite - commonly associated with volcanic glass. Some lining of vesicles.
(3-4%) Quartz - small, anhedral, often found in vesicles.
(5%) Fe-oxides - anhedral, interstitial, hematite staining is common.

$FeO/Fe_2O_3 = 1.02$

Sample S-19

(40%) Plagioclase - An_{52} (Michel Lèvy), 0.421 (C.I.P.W. albite ratio).
(20%) Augite - small, anhedral. Some larger phenocrysts.
(2-3%) Hypersthene - anhedral to subhedral, altering to groundmass.
(18%) Volcanic Glass - fractured, devitrified, numerous microphenocrysts.
(7-8%) Chlorite - often lining vesicles, some interstitial.
(2-3%) Quartz - anhedral, interstitial. Often infilling vessels.
(7-8%) Fe-oxides - small, anhedral, minor hematite staining.
$FeO/Fe_2O_3 = 0.61$

Sample T-20

(40%) Plagioclase - An_{54} (Michel Lèvy), 0.465 (C.I.P.W. albite ratio).
(15%) Augite - small, anhedral. Some larger phenocrysts.
(2-3%) Hypersthene - anhedral to subhedral, altering to groundmass.
(29%) Volcanic Glass - devitrified, reddish-brown. Numerous microphenocrysts.
(5%) Chlorite - interstitial, occasionally lining vesicles.
(2-3%) Quartz - small, anhedral.
(5%) Fe-oxides - small, anhedral, minor hematite staining.
$FeO/Fe_2O_3 = 0.35$

Sample U-21

(35%) Plagioclase - An_{52} (Michel Lèvy), 0.526 (C.I.P.W. albite ratio).
(20%) Augite - small, anhedral, colour zoning of crystals.
(1-2%) Hypersthene - small, anhedral. Some rare large, subhedral phenocrysts.
(32%) Volcanic Glass - devitrified, numerous microphenocrysts, reddish-brown.
(5%) Chlorite - interstitial, often associated with plagioclase crystals.
(2-3%) Quartz - small, anhedral. Often found infilling vesicles.
(2-3%) Fe-oxides - large, anhedral. Some interstitial, minor hematite staining.
$FeO/Fe_2O_3 = 0.27$

Sample V-22

(45%) Plagioclase - An_{59} (Michel Lèvy), 0.412 (C.I.P.W. albite ratio).
(20%) Augite - small, subhedral. Some larger phenocrysts.
(5%) Hypersthene - small, anhedral. Commonly found interstitially.
(8%) Volcanic Glass - devitrified, reddish-brown.
(10%) Chlorite - interstitial with volcanic glass. Some lining of vesicles.
(3-4%) Quartz - small, subhedral.
(7-8%) Fe-oxides - anhedral, large, minor hematite staining.
FeO/Fe_2O_3 = 1.12

Sample W-23

(35%) Plagioclase - An_{59} (Michel Lèvy), 0.349 (C.I.P.W. albite ratio).
(15%) Augite - subhedral, commonly colour zoned.
(2-3%) Hypersthene - small, anhedral. Some larger phenocrysts.
(30%) Volcanic Glass - devitrified, interaction with surrounding crystals.
(7-8%) Chlorite - commonly associated with the volcanic glass.
(3-4%) Quartz - subhedral to euhedral. Commonly infilling vesicles.
(5%) Fe-oxides - small, anhedral, interstitial. Some larger xenoblasts.
FeO/Fe_2O_3 = 0.54

Sample X-24

(40%) Plagioclase - An_{55} (Michel Lèvy), 0.437 (C.I.P.W. albite ratio).
(15%) Augite - subhedral, colour zoning of crystals is common.
(5%) Hypersthene - small, anhedral, interstitial.
(29%) Volcanic Glass - devitrified, reddish-brown.
(5%) Chlorite - commonly associated with volcanic glass.
(2-3%) Quartz - small, subhedral.
(2-3%) Fe-oxides - small, anhedral, interstitial.
FeO/Fe_2O_3 = 0.20.

Sample Y-25

(35%) Plagioclase - An_{57} (Michel Lèvy), 0.376 (C.I.P.W. albite ratio).
(15%) Augite - subhedral, crystals are often colour zoned.
(2-3%) Hypersthene - small, anhedral, altering to groundmass.
(31%) Volcanic Glass - devitrified, commonly altering associated minerals.
(7-8%) Chlorite - commonly lining vesicles, spherulites are common.
(2-3%) Quartz - subhedral, interdigitating boundaries (solution effect).
(2-3%) Fe-oxides - anhedral, hematite staining is common.
$FeO/Fe_2O_3 = 0.45$

Sample Z-26

(40%) Plagioclase - An_{57} (Michel Lèvy), 0.439 (C.I.P.W. albite ratio).
(20%) Augite - small, subhedral, often colour zoned.
(2-3%) Hypersthene - small, anhedral, altering to groundmass.
(18%) Volcanic Glass - devitrified, numerous microphenocrysts.
(7-8%) Chlorite - interstitial, often found associated with volcanic glass.
(2-3%) Quartz - small, anhedral, fractured. Commonly interstitial.
(7-8%) Fe-oxides - anhedral, hematite staining is common.
$FeO/Fe_2O_3 = 0.72$

Note

To approximate the relative proportions of minerals observed in thin sections by visual inspection is relatively inaccurate, especially when dealing with rocks that are considerably altered. Further research projects may include more elaborate methods in determining modal compositions such as point counting techniques.

Volcanic glass is an all encompassing term used in this appendix which includes true volcanic glass, finely crystalline groundmass, microphenocrysts and alteration products. This component was extremely difficult to estimate due to its variable nature in this suite of rocks. Therefore, true volcanic glass should not be confused with this term as it comprises only a portion of this total.

REFERENCES

1. Bailey et al., 1924, pp. 141-43. Fawcett, J.J., (1965) Alteration products of olivine and pyroxene in basalt lavas from the Isle of Mull. Miner. Mag. 35, 55-68.

2. Baker, Charles Laurence (1922), The lava fields of the Paraná Basin, South American, Trans. Geol. Soc. South Africa, Vol. xxiii, pp. 1-42.

3. Barker, Daniel S. (1983), Igneous Rocks, Prentice-Hall, Inc., Englewood Cliffs, N.J.

4. Basaltic Volcanism Study Project (1981), Basaltic Volcanism on the terrestrial planets. Pergamon Press, Inc., New York. 1286 pp.

5. Birch, F. and P. LeComte (1960), Temperature-pressure plane for albite composition, Am. J. Sci., 258, 209-217.

6. Bowen, N.L. (1928), The evolution of the igneous rocks, Princeton University Press, Princeton, New Jersey, 332p.

7. Boyd, F.R., and P.H. Nixon (1973), Structure of the upper mantle beneath Lesotho, Carnegie Inst. Washing Yearb. 72, 431-445.

8. Carmichael, I.S.E., Turner, F.J., Verhoogen, J. (1974), Igneous Petrology, International Series in the Earth and Planetary Sciences. McGraw-Hill, Inc., U.S.A.

9. Cordani, U.G. and Vandoros, P. (1967), Basaltic rocks of the Paraná Basin. In problems in Brazilian Gondwana stratigraphy and paleontology, Mar del Plata, pp. 207-31. Int. Symp. Godwana Stratig. Paleont. 1st Mar del Plata. Curitiba, Brazil.

10. Davis, B.T.C., and F.R. Boyd (1966), The join $Mg_2Si_2O_6$-$CaMgSi_2O_6$ at 30 kilobars pressure and its application to pyroxenes from Kimberlites, J. Geophys. Res., pp. 3567-3576.

11. Deer, W.A. and R.A. Howie, and J. Zussman (1966), An introduction to the rock-forming minerals, Longman Group Limited, Burnt Mill, Harlow, Essex, England.

12. Ehlers, Ernest G. and Harvey Blatt (1980), Petrology: igneous, sedimentary and metamorphic, W.H. Freeman and Company, U.S.A.

13. Ito, K., and G.C. Kennedy (1967), Melting and phase relations in a natural peridotite to 40 kilobars, Am. J.

14. Kerr, Paul F. (1977), Optical Mineralogy, McGraw-Hill Inc., New York.

15. Kushiro, I. (1968), Compositions of magmas formed by partial zone melting of the earths upper mantle, J. Geophys. Res., 73, 619-634.

16. Kushiro, I. (1969), Clinopyroxene solid solutions formed by reactions between diopside and plagioclase at high pressures, Miner. Soc. Am. Spec. Pap. 2, 179-91.

17. Kushiro, I. (1969), The system forsterite-diopside-silica with and without water at high pressures, Am. J. Sci., Schairer Vol., 267A, 269-294.

18. Kushiro, I. (1972), Determination of liquidus relations in synthetic silicate systems with electron probe analysis: the system forsterite-diopside-silica at 1 atmosphere, Am. Mineral., 57, 1260-1271.

19. Kushiro, I. (1972), Effect of water on the compositions of magmas formed at high pressures, J. Petrol., 13, 311-334.

20. Kushiro, I. (1973), Origin of some magmas in oceanic and circum-oceanic regions, Tectonophysics, 17, 211-222.

21. Kushiro, I. (1973), Partial melting of garnet lherzolites from Kimberlite at high pressures. In P.H. Nixon, ed., Lesotho National Development Corporation, Maseru, Lesotho, pp. 294-299.

22. Kushiro, I. and H.S. Yoder, Jr. (1966), Anorthite-forsterite and anorthite-enstatite reactions and their bearing on the basalt-eclogite transformation, J. Petrol., 7, 337-362.

23. Maack, R. (1952), Die eintwicklung der Gondwana Schicten Suedbrasilien und ihre Beziehungen zur Karru-Formation Suedafrikas., Int. Geol. Congr., 19, Algiers, Sympos. sur les Series de Gondwana, 339-372.

24. MacGregor, I.D. (1974), The system $MgO-Al_2O_3-SiO_2$: solubility of Al_2O_3 in enstatite from spinel and garnet peridotite compositions, Am. Mineral., 59, 110-119.

25. Maxwell, J.A. (1968), Rock and mineral analysis, Interscience Publishers, John Wiley, New York.

26. Morse, S.A. (1980), Basalts and phase diagrams, Springer-Verlag Inc., New York.

27. Mysen, B.O. (1976), Experimental determination of some geochemical parameters relating to conditions of equilibration of peridotite in the upper mantle, Am. Mineral., 61, 677-683.

28. Mysen, B.O. (1976), Partioning of samarium and nickel between olivine, orthopyroxene and liquid: preliminary data at 20 kilobars and 1025°C, Earth Planet. Sci. Lett., 31, 1-7.

29. Nockolds, S.R., and R.W. O'B. Knox, and G.A. Chinner (1978), Petrology for students, Cambridge University Press, Cambridge.

30. Robie, R.A. and B.S. Hemingway, and J.R. Fischer (1978), Thermodynamic properties of minerals and related substances at 298.15K and 1 bar (10^5 pascals) pressure and at higher temperatures. U.S. Geol. Surv. Bull. 1452.

31. Schairer, J.F., and H.S. Yoder, Jr. (1964), Crystal and liquid trends in simplified alkali basalts, Carnegie Inst. Washington Yearb. 63, 65-74.

32. Valencio, Daniel Alberto (1972), Paleomagnetism of the lower Cretaceous Vulcanitas Cerro Colorado Formation of the Sierra De Los Condores Group Province of Cordoba, Argentina, Earth and Planetary Science Letters 16 (1972), North-Holland Publishing Company.

33. Wilshire, H.G., and J.W. Shervais (1975), Al-augite and Cr-diopside ultramafic xenoliths in basaltic rocks from western United States, Phys. Chem, Earth, 9, 257-272.

34. Yoder, H.S. Jr. (1976), Generation of basaltic magma, National Academy of Sciences, Washington, D.C.

BASE MAP OF THE MISIONES PROVINCE, ARGENTINA

PARAGUAY

POSADAS

A-01
GARUPA
J-10
Q-17
STA. ANA
SAN IGNACIO
R-18

rio parana

K-11
H-08
GARUHAPE
Z-26
Y-25
O-15
ELDORADO
U-21
I-09

C-03
SAN MARTIN CATARATAS
V-22
rio iguazu
F-06
a. aguaray mini
a. piray mini
a. piray guazu
a. paranay guazu
NORTH

a. garabi
X-24
GENERAL GÜEMES
APOSTOLES
AZARA
L-12
S-19
N-14
GARRUCHOS
M-13
T-20
B-02
GARRUCHOS
CONCEPCION
ALEM
D-04
W-23
P-16
E-05
OBERA
CAMPO GRANDE
MISIONES
SAN PEDRO
G-07

SAN JAVIER
XAVIER
PANAMBI
ALBA
POSSE
rio uruguay
BRAZIL
EL SOBERBIO
rio pepiri guazu

LEGEND

● CITIES

\+ SAMPLE LOCATION

SCALE

0 10 20 30 40 60 km